J|A|C|S ARTICLES

Published on Web 03/30/2009

Interaction of Organoplatinum(II) Complexes with Monovalent Coinage Metal Triflates

Marc-Etienne Moret and Peter Chen*

Laboratorium für Organische Chemie, Eidgenössische Technische Hochschule (ETH) Zürich, CH-8093 Zürich, Switzerland

Received January 20, 2009; E-mail: peter.chen@org.chem.ethz.ch

Abstract: The organoplatinum(II) complexes [(NN)$PtMe_2$] and [(NN)$PtPh_2$] (NN = ArNC(Me)C(Me)NAr, Ar = 2,6-dichlorophenyl) can act as donor ligands for copper(I) and silver(I) triflates, affording a series of homo- and heteroleptic complexes which were characterized by X-ray diffraction. [(NN)$PtMe_2$] binds to the coinage metals through short, ligand-unsupported d−d^{10} contacts that are best described as Pt→M dative bonds (M = Cu, Ag), in which the d_{z^2} orbital of the square-planar Pt(II) center donates electron density to the Lewis-acidic metal. Spectroscopic studies in solution and DFT calculations corroborate this description. [(NN)$PtPh_2$] binds preferentially by η^1 or η^2 complexation of the *ipso* carbon atoms of the phenyl groups to the coinage metal, affording homoleptic complexes $\{[(NN)PtPh_2]_2M\}^+\{TfO\}^-$ in the solid state. The 1:1 adducts of formula $\{[(NN)PtPh_2]M(OTf)\}_n$ (M = Cu, n = 1; M = Ag, n = 2) are observed in solution, and a 1:2 adduct of formula $\{[(NN)PtPh_2]Ag_2(OTf)_2(C_6H_6)\}_n$ was characterized in the solid state, showing that unsupported Pt→M bonds are also accessible for [(NN)$PtPh_2$]. The thermolyses of the complexes [(NN)$PtMe_2$]MOTf in benzene affords moderate yields of [(NN)$PtPh_2$] through an oxidatively induced double C−H activation process.

Introduction

Metallophilic bonds, i.e. attractive interactions between closed shell transition metals, are a topic of increasing interest, due both to the theoretical challenge of accurately describing them,[1−6] and to their practical utility. The latter includes their use as a tool for crystal engineering[7,8] and for the design of luminescent compounds.[9−11] Square-planar d^8 complexes can be regarded as closed-shell species due to the strong ligand-field splitting of the d orbitals,[1] and thus can be involved in metallophilic bonds. In fact, d^8−d^{10} interactions have been found in a variety of compounds.[12−18]

A particular case of d^8−d^{10} interactions is constituted by the bonds formed between an electron-rich platinum(II) center and a Lewis-acidic coinage metal, which are thought to have a significant donor−acceptor character and thus are often referred to as Pt→M dative bonds. This kind of bonding has been found in a broad range of compounds for M = Ag(I),[9,19−34] but is also known for M = Au(I).[9,33−36] For example, Yamagushi et al. [29] reported an interesting one-dimensional metal chain built from Pt→Ag bonds, and compounds featuring Pt→Ag bonds

(1) Pyykkö, P. *Chem. Rev.* **1997**, *97*, 597–636.
(2) Hermann, H. L.; Boche, G.; Schwerdtfeger, P. *Chem.-Eur. J.* **2001**, *7*, 5333–5342.
(3) Xia, B.-H.; Zhang, H.-X.; Jiao, Y.-Q.; Pan, Q.-J.; Li, Z.-S.; Sun, C.-C. *J. Chem. Phys.* **2004**, *120*, 11487–11492.
(4) Pyykkö, P.; Patzschke, M. *Faraday Discuss.* **2003**, *124*, 41–51.
(5) Zhang, J.-P.; Wang, Y.-B.; Huang, X.-C.; Lin, Y.-Y.; Chen, X.-M. *Chem.-Eur. J.* **2005**, *11*, 552–561.
(6) Poblet, J.-M.; Bénard, M. *Chem. Commun.* **1998**, 1179–1180.
(7) Katz, M. J.; Sakai, K.; Leznoff, D. B. *Chem. Soc. Rev.* **2008**, *37*, 1884–1895.
(8) Zheng, X.-D.; Jiang, L.; Feng, X.-L.; Lu, T.-B. *Inorg. Chem.* **2008**, 47.
(9) Yip, H.-K.; Lin, H.-M.; Cheung, K.-K.; Che, C.-M.; Wang, Y. *Inorg. Chem.* **1994**, *33*, 1644–1651.
(10) Gil, B.; Forniés, J.; Gómez, J.; Martín, A.; Moreno, M. T. *Inorg. Chem.* **2006**, *45*, 7788–7798.
(11) Fernández, E. J.; Laguna, A.; de Luzuriaga, J. M. L. *Dalton Trans.* **2007**, 1969–1981.
(12) Balch, A. L.; Catalano, V. J. *Inorg. Chem.* **1991**, *30*, 1302–1308.
(13) Heckenroth, M.; Kluser, E.; Neels, A.; Albrecht, M. *Angew. Chem., Int. Ed.* **2007**, *46*, 6293–6296.
(14) Crespo, O.; Laguna, A.; Fernández, E. J.; de Luzuriaga, J. M. L.; Jones, P. G.; Teichert, M.; Monge, M.; Pyykkö, P.; Runeberg, N.; Schütz, M.; Werner, H. J. *Inorg. Chem.* **2000**, *39*, 4786–4792.
(15) Balch, A. L.; Catalano, V. J.; Olmstead, M. M. *Inorg. Chem.* **1990**, *29*, 585–586.
(16) Kim, M.; Taylor, T. J.; Gabbai, F. P. *J. Am. Chem. Soc.* **2008**, *130*, 6332–6333.
(17) Kickham, J. E.; Loeb, S. J. *Organometallics* **1995**, *14*, 3584–3587.
(18) Yamaguchi, T.; Yamazaki, F.; Ito, T *J. Am. Chem. Soc.* **1999**, *121*, 7405–7406.
(19) Baudron, S. A.; Hosseini, M. W. *Chem. Commun.* **2008**, 4558–4560.
(20) Janzen, D. E.; Mehne, L. F.; vanDerveer, D. G.; Grant, G. J. *Inorg. Chem.* **2005**, *44*, 8182–8184.
(21) Song, H. B.; Zhang, Z.-Z.; Hui, Z.; Che, C.-M.; Mak, T. C. W. *Inorg. Chem.* **2002**, *41*, 3146–3154.
(22) Kampf, G.; Miguel, P. J. S.; Willermann, M.; Schneider, A.; Lippert, B. *Chem.-Eur. J.* **2008**, *14*, 6882–6891.
(23) Forniés, J.; Martínez, F.; Navarro, R.; Urriolabeitia, E. P. *Organometallics* **1996**, *15*, 1813–1819.
(24) Usón, R.; Forniés, J.; Menjón, B.; Cotton, F. A.; Falvello, L. R.; Tomás, M. *Inorg. Chem.* **1985**, *24*, 4651–4656.
(25) Uson, R.; Forniés, J.; Tomás, M.; Cotton, F. A.; Falvello, L. R. *J. Am. Chem. Soc.* **1984**, *106*, 2482–2483.
(26) Forniés, J.; Navarro, R.; Tomás, M.; Urriolabeitia, E. P. *Organometallics* **1993**, *12*, 940–943.
(27) Forniés, J.; Fortuño, C.; Ibáñez, S.; Martín, A. *Inorg. Chem.* **2008**, *47*, 5978–5987.
(28) Forniés, J.; Ibáñez, S.; Martín, A.; Sanz, M.; Berenguer, J. R.; Lalinde, E.; Torroba, J. *Organometallics* **2006**, *25*, 4331–4340.
(29) Yamagushi, T.; Yamazaki, F.; Ito, T. *J. Am. Chem. Soc.* **2001**, *123*, 743–744.

have been found to be intermediates for halogen abstraction reactions on platinum(II).[27] Of particular relevance to this work is the observation by the group of Puddephatt[34] of the sandwich complex $\{[(bpy)PtMe_2]_2Ag\}^+\{BF_4\}^-$ (bpy = 2,2′-bipyridyl) at low temperature. This complex was found to undergo reversible Pt−Me bond cleavage at −40 °C, but decomposes with precipitation of Ag(0) when allowed to warm to room temperature. Only a few compounds are known that incorporate Pt→Cu(I) bonds,[19,21,33,35] and to our knowledge, the metal−metal interaction is supported by bridging ligands in all cases. We recently reported compounds featuring a Pt_2Cu_2 core in which the central copper(I) atom is held only by a cuprophilic interaction and two Pt→Cu bonds.[37]

Compounds of general formula $[(NN)PtR_2]$ (NN = α-diimine ligand, R = Me, Ph) have attracted much attention because of their use as precursors in C−H activation reactions.[38−51] Upon activation with a Brønsted acid, they eliminate one equivalent of methane or benzene and generate active species with a weakly bound solvent molecule or counteranion that can be exchanged for an alkane or arene in the first step of the C−H activation process. A subsequent oxidative addition/reductive elimination sequence then generates methyl and phenyl complexes from methane and benzene, respectively. A slightly more complex reaction yields dehydrogenation products from higher alkanes.[52] The initial ligand exchange is often rate determining,[46] and thus the absence of strong ligands in the reaction mixture is critical.

The α-diimine ligand **1** (Scheme 1) has previously been used in our group to stabilize reactive intermediates relevant to C−H bond activation in mass spectrometric studies.[53−56] The dimethyl-[53] and diphenylplatinum(II)[56] complexes **2** and **3** are readily

Scheme 1

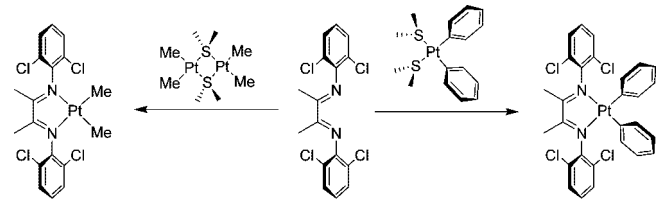

accessible through the reaction of **1** with suitable precursors (Scheme 1). We set out to study the interaction of **2** and **3** with coinage metal triflates with a two-fold objective: (1) to access structurally simple compounds featuring Pt→Ag and Pt→Cu bonds in order to allow a better characterization of this kind of binding, and (2) to probe whether these interactions would alter the chemical properties of the Pt−R bonds and give access to novel reactivity in relation with C−H bond activation. We reasoned that the *ortho*-dichlorophenyl groups of ligand **1** would at the same time offer some steric protection against aggregation and, by withdrawing electron density from the diimine moiety, render the complexes more robust toward the above-mentioned oxidative decomposition reported by Puddephatt.[34]

In this contribution, we first report the solid-state characterization of a series of compounds featuring ligand-unsupported Pt→Cu and Pt→Ag bonds. Then, we present the study of these interactions in solution by a range of spectroscopic techniques, and discuss their nature on the basis of density functional theory (DFT) calculations. Finally, we describe an oxidatively induced double C−H activation reaction which transforms **2** into **3** in the presence of CuOTf or AgOTf in benzene.

Results and Discussion

Solid-State Studies. The interaction of the dimethylplatinum(II) complex **2** and its diphenyl analogue **3** with monovalent coinage metal triflates was first studied by preparing crystals of the corresponding adducts and analyzing them by X-ray diffraction (XRD). The compounds involving **2** are discussed first.

The addition of $CuOTf \cdot 1/2C_7H_8$ to a dark-green solution of **2** in toluene yielded a clear, dark-red solution from which the 1:1 adduct **4a** could be isolated in 46% yield (Scheme 2). Compound **4a** slowly decomposes at room temperature in aromatic solvents (*vide infra*), but crystals suitable for XRD could be obtained from a benzene/hexane mixture at −35 °C.

The most striking feature in the crystal structure of **4a** (Figure 1) is the ligand-unsupported Pt−Cu bond. With 2.3992(16) Å, it is markedly shorter than sum of the covalent radii (1.36(Pt) + 1.32(Cu) = 2.68 Å),[57] and, to the best of our knowledge, it is the shortest Pt−Cu contact reported to date. The Pt−Cu bond makes an angle of 81° with the coordination plane of the platinum center, which supports its description as a Pt→Cu dative bond involving donation of electron density from the filled d_{z^2} orbital of Pt(II) to the Lewis-acidic Cu(I) ion. Thus, the Pt(II)

(30) Uson, R.; Fornies, J.; Tomas, M.; Casas, J. M.; Cotton, F. A.; Falvello, L. R.; Llusar, R. *Organometallics* **1988**, *7*, 2279–2285.
(31) Usón, R.; Forniés, J.; Tomás, M.; Ara, I.; Casas, J. M.; Martin, A. *J. Chem. Soc., Dalton Trans.* **1991**, 2253–2264.
(32) Usón, R.; Forniés, J. *Inorg. Chim. Acta* **1992**, *198−200*, 165–177.
(33) Xia, B.-H.; Zhang, H.-X.; Che, C.-M.; Leung, K.-H.; Phillips, D.-L.; Zhu, N.; Zhou, Z.-Y. *J. Am. Chem. Soc.* **2003**, *125*, 10362–10374.
(34) Arsenault, G. J.; Anderson, C. M.; Puddephatt, R. J. *Organometallics* **1988**, *7*, 2094–2097.
(35) Yin, G.-Q.; Wei, Q.-H.; Zhang, L.-Y.; Chen, Z.-N. *Organometallics* **2006**, *25*, 580–587.
(36) Yip, H.-K.; Lin, H.-M.; Wang, Y.; Che, C.-M. *J. Chem. Soc., Dalton Trans.* **1993**, 2939–2944.
(37) Moret, M.-E.; Chen, P. *Organometallics* **2008**, *27*, 4903–4916.
(38) Johannsson, L.; Ryan, O. B.; Tilset, M. *J. Am. Chem. Soc.* **1999**, *121*, 1974–1975.
(39) Wik, B. J.; Lersch, M.; Krivokapic, A.; Tilset, M. *J. Am. Chem. Soc.* **2006**, *128*, 2682–2696.
(40) Heiberg, H.; Johansson, L.; Gropen, O.; Ryan, O. B.; Swang, O.; Tilset, M. *J. Am. Chem. Soc.* **2000**, *122*, 10831–10845.
(41) Lersch, M.; Tilset, M. *Chem. Rev.* **2005**, *105*, 2471–2526.
(42) Johansson, L.; Ryan, O. B.; Rømming, C.; Tilset, M. *J. Am. Chem. Soc.* **2001**, *123*, 6579–6590.
(43) Gerdes, G.; Chen, P. *Organometallics* **2004**, *23*, 3031–3036.
(44) Gerdes, G.; Chen, P. *Organometallics* **2006**, *25*, 809–811.
(45) Labinger, J. A.; Bercaw, J. E.; Tilset, M. *Organometallics* **2006**, *25*, 808–808.
(46) Johansson, L.; Tilset, M.; Labinger, J. A.; Bercaw, J. E. *J. Am. Chem. Soc.* **2000**, *122*, 10846–10855.
(47) Zhong, H. A.; Labinger, J. A.; Bercaw, J. E. *J. Am. Chem. Soc.* **2002**, *124*, 1378–1399.
(48) Driver, T. G.; Day, M. W.; Labinger, J. A.; Bercaw, J. E. *Organometallics* **2005**, *24*, 3644–3654.
(49) Driver, T. G.; Williams, T. J.; Labinger, J. A.; Bercaw, J. E. *Organometallics* **2007**, *26*, 294–301.
(50) Williams, T. J.; Caffyn, A. J. M.; Hazari, N.; Oblad, P. F.; Labinger, J. A.; Bercaw, J. E. *J. Am. Chem. Soc.* **2008**, *130*, 2418–2419.
(51) Owen, J. S.; Labinger, J. A.; Bercaw, J. E. *J. Am. Chem. Soc.* **2006**, *128*, 2005–2016.
(52) Chen, G. S.; Labinger, J. A.; Bercaw, J. E *Proc. Natl. Acad. Sci. U.S.A.* **2007**, *104*, 6915–6920.
(53) Hammad, L. A.; Gerdes, G.; Chen, P. *Organometallics* **2005**, *24*, 1907–1913.
(54) Gerdes, G.; Chen, P. *Organometallics* **2003**, *22*, 2217–2225.
(55) Moret, M.-E.; Chen, P. *Organometallics* **2007**, *26*, 1523–1530.
(56) Gerdes, G. Thesis, Catalytic C-H activation of benzene by platinum(II): a mechanistic study, ETHZ, 2004.
(57) Cordero, B.; Gómez, V.; Platero-Prats, A. E.; Revés, M.; Echeverría, J.; Cremades, E.; Barragán, F.; Alvarez, S. *Dalton Trans.* **2008**, 2832–2838.

Scheme 2

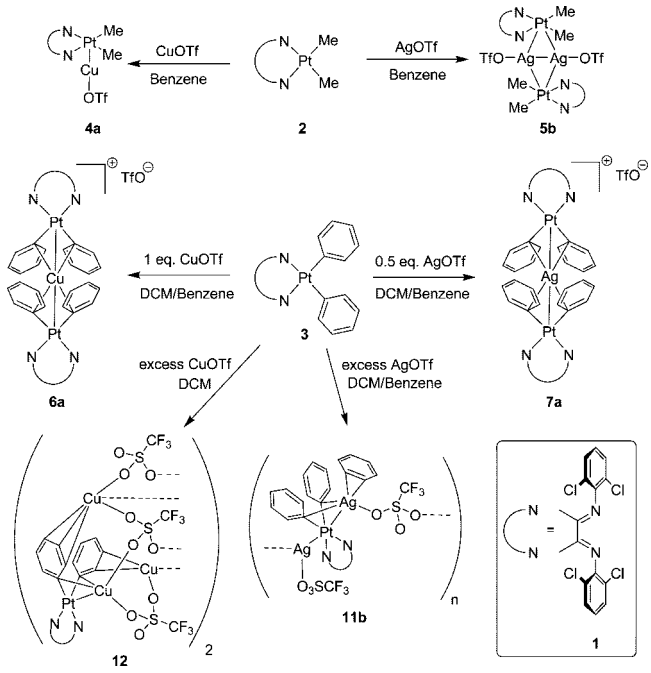

complex can be considered as a σ-donor ligand. The coordination around the Cu(I) center is then best described as a linear, two-coordinate environment involving the Pt(II) complex and the η^1 triflate anion as ligands. Comparison with the structure of **2**[53] reveals a slight lengthening of the Pt−C (2.032(11) and 2.039(13) vs 2.007(7) Å) and Pt−N bonds (2.100(9) and 2.110(10) vs 2.076(5) Å) upon coordination to Cu(I), suggesting that these bonds are somewhat weakened.

The silver analogue of **4a** was prepared in 64% yield by reaction of **2** with AgOTf in benzene (Scheme 2). Analysis of the dark-red crystals by XRD revealed the formation of the centrosymmetric 2:2 adduct **5b** (Figure 2). The crystal structure of **5b** exhibits a planar Pt_2Ag_2 core built from four unsupported Pt→Ag bonds (2.8290(6) and 2.9097(5) Å) and an argentophilic interaction (2.6972(2) Å). This core structure is similar to that of the known compound $(NBu_4)_2[Pt_2Ag_2Cl_4(C_6F_5)_4]$, which is however additionally stabilized by four bridging chloride anions and weak ArF−Ag contacts.[24,25] The influence of two silver(I) ions on the coordination environment of platinum(II) is stronger than that of a single copper(I) ion, as indicated by somewhat longer Pt−C (2.039(4) and 2.043(4) Å) and Pt−N bonds (2.117(3) and 2.118(3) Å) in **5b** than in **4a**, and by a slight displacement of the Pt atom out of the plane of the ligands in **5b** (0.17 Å from the best C_2N_2 plane). The fact that a dimeric structure is observed for **5b** and not for **4a** supports the idea that argentophilic interactions are stronger than cuprophilic interactions.[2,5]

The bonding situation becomes different when the complexes of the diphenyl complex **3** are considered. The reaction of **3** with 0.55 equiv of $CuOTf \cdot 1/2C_7H_8$ in dichloromethane yielded a dark-purple solution, from which the 2:1 adduct **6a** could be crystallized as black needles (52%) by addition of toluene followed by slow concentration. The XRD study of **6a** (Figure 3) reveals an ionic structure containing a free triflate anion and a homoleptic 2:1 complex cation, which possesses a C_2 rotation axis. While the Pt−Cu distance (2.7254(3) Å) is relatively short, the very acute angle (25°) between the coordination plane of the Pt center and the Pt−Cu axis presumably does not allow

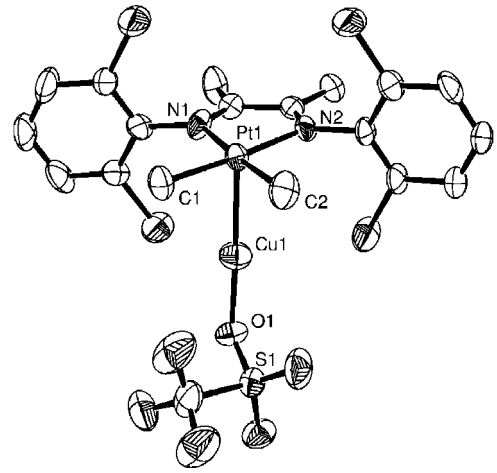

Figure 1. ORTEP representation of the X-ray crystal structure of **4a**. Ellipsoids are drawn at 50% probability. Selected distances [Å] and angles [deg]: Pt1−Cu1 2.3992(16), Cu1−O1 1.907(8), Pt1−C1 2.032(11), Pt1−C2 2.039(13), Pt1−N1 2.110(10), Pt1−N2 2.100(9), O1−Cu1−Pt1 175.4(3), C1−Pt1−C2 87.4(6), C1−Pt1−N1 98.3(5), C2−Pt1−N2 98.6(5), N1−Pt1−N2 75.6(4), C1−Pt1−Cu1 82.3(4), C2−Pt1−Cu1 84.8(4), N1−Pt1−Cu1 95.1(3), N2−Pt1−Cu1 98.4(3), Cu1−O1−S1 121.7(5).

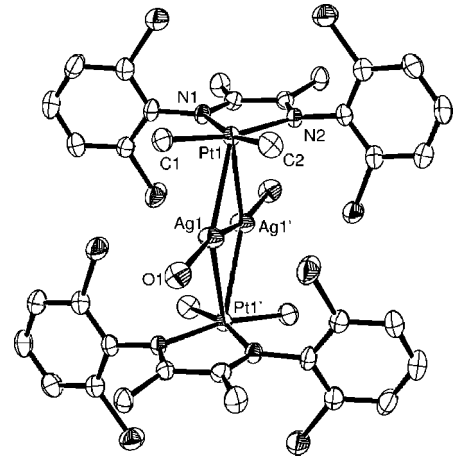

Figure 2. ORTEP representation of the X-ray crystal structure of **5b**. Ellipsoids are drawn at 50% probability. For clarity, only the silver-bound oxygen atom of the $CF_3SO_3^-$ units is plotted, and an unbound benzene molecule is omitted. Selected distances [Å], angles [deg], and torsion angles [deg]: Ag1−Ag1′ 2.6972(2), Ag1−O1 2.354(3), Ag1−Pt1 2.8290(6), Ag1−Pt1 2.9097(5), Pt1−C1 2.039(4), Pt1−C2 2.043(4), Pt1−N1 2.117(3), Pt1−N2 2.118(3), Ag1′−Ag1−Pt1 63.489(15), Ag1−Pt1−Ag1′ 56.047(15), O1−Ag1′−Ag1 164.82(8), C1−Pt1−C2 89.28(17), C1−Pt1−N1 97.19(14), C2−Pt1−N2 96.28(14), N1−Pt1−N2 75.59(11), Pt1−Ag1−Ag1′−Pt1′ 180.0.

for a significant donation of electron density from the d_{z^2} orbital of Pt(II) to the Cu(I) cation. Thus, the Pt−Cu interaction is expected to consist mainly of dispersion forces and, consequently, to be weaker than in **4a**. However, this fact is compensated by a close contact (2.138(5) Å) and a more distant one (2.336(5) Å) between the Cu(I) center and the *ipso* carbon atoms of the phenyl ligands. These interactions are also reflected by the tilting of the phenyl rings, shown by the nonzero values of the Pt−C3−C4−C1 (7.9 °) and Pt−C5−C6−C2 (−7.8 °) dihedral angles. Additionally, the Pt−C bonds are somewhat longer than those in the free platinum complex **3**[56] (2.022(5) and 2.033(5) vs 2.003(3) and 2.004(4) Å).

The similar 2:1 silver adduct **7a** could be obtained in 61% yield from the reaction of **3** with AgOTf. However, all the conditions we applied yielded severely disordered crystals. The

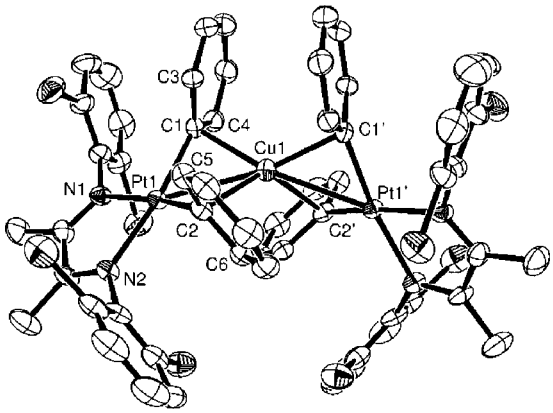

Figure 3. ORTEP representation of the X-ray crystal structure of the cation of **6a**. Ellipsoids are drawn at 50% probability. The disordered, unbound $CF_3SO_3^-$ counterion is omitted for clarity. Selected distances [Å], angles [deg], and torsion angles [deg]: Cu1−Pt1 2.7254(3), Cu1−C1 2.138(5), Cu1−C2 2.336(5), Pt1−C1 2.033(5), Pt1−C2 2.022(5), Pt1−N1 2.106(5), Pt1−N2 2.082(4), Pt1−Cu1−Pt1′ 144.86(4), Pt1−Cu1−C1 47.55(13), Pt1−Cu1−C2 46.31(12), C1−Cu1−C2 82.60(18), C1−Cu1−C1′ 126.3(3), C2−Cu1−C2′ 130.4(3), C1−Cu1−C2′ 120.50(17), C1−Pt1−C2 93.64(18), C1−Pt1−N1 95.47(17), C2−Pt1−N2 95.07(17), N1−Pt1−N2 75.37(15), Pt1−C3−C4−C1 7.9, Pt1−C5−C6−C2 −7.8.

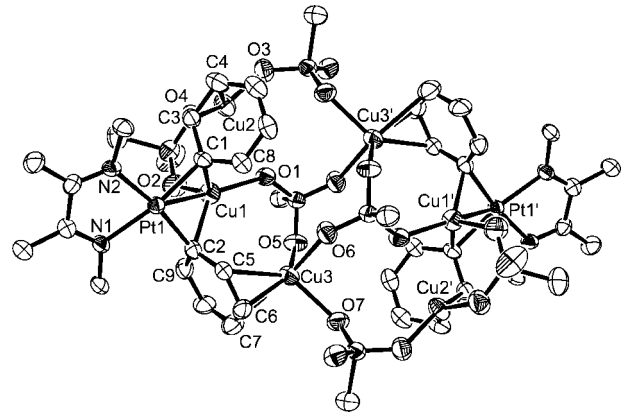

Figure 4. ORTEP representation of the centrosymmetric molecular unit of **12**. Ellipsoids are drawn at 50% probability. The aromatic groups of the diimine ligand, the fluorine atoms of the CF_3SO_3 units, and six CH_2Cl_2 solvent molecules are omitted for clarity. Selected distances [Å], angles [deg], and torsion angles [deg]: Cu1−Pt1 2.5995(8), Pt1−C1 2.048 (5), Pt1−C2 2.028(6), Pt1−N1 2.097(5), Pt1−N2 2.097(5), Cu1−C1 2.160(5), Cu1−C2 2.146(6), Cu1−O1 2.083(5), Cu1−O2 2.123(5), Cu2−C3 2.112(6), Cu2−C4 2.148(7), Cu2−O3 2.034(5), Cu2−O4 2.077(5), Cu3−C5 2.484(7), Cu3−C6 2.069(7), Cu3−C7 2.412(9), Cu3−O5 2.079(5), Cu−O6 2.148(5), Cu3−O72.177(5), C1−Pt1−C293.8(2), Pt1−C3−C8−C1 10.1, Pt1−C5−C9−C2 9.8.

XRD data (see Supporting Information) is good enough, though, to confirm that **7a** is isostructural with **6a** and to measure a Pt−Ag distance of 3.28 Å, which indicates a weak (if any) d^8-d^{10} interaction, the bonding consisting mainly of the coordination of the phenyl rings to the silver cation.

As solution-phase UV−vis and ^{1}H NMR spectroscopic data (*vide infra*) indicated the existence of species with a different stoichiometry than that found in **6a** and **7a**, we explored crystallization conditions with a higher CuOTf:**3** or AgOTf:**3** ratio. At a 1:1 ratio, only crystals of **6a** and **7a**, respectively, were obtained.

In most crystallization attempts involving higher CuOTf:**3** ratios, the low solubility of CuOTf caused it to precipitate together with the platinum containing compound(s), and the obtained residues were unsuitable for both XRD and elemental analysis. However, saturation of a solution of **3** in dichloromethane with CuOTf·C_6H_6 followed by slow cooling afforded a small amount of the 2:6 adduct **12** as dark-purple needles. XRD analysis (Figure 4) shows that the molecular unit of **12** consists of a centrosymmetric, hexanuclear Cu(I) triflate cluster stabilized by interaction with two (NN)$PtPh_2$ units. One of the three crystallographically independent Cu(I) centers (Cu1) is bound to the (NN)$PtPh_2$ moiety in a similar fashion to that found in compound **6a**, with slightly shorter contacts with the *ipso* carbon atoms of the phenyl groups (2.160(5) and 2.146(6) vs 2.138(5) and 2.336(5) Å) and with the platinum center (2.5995(8) vs 2.7254(3)). The two other Cu(I) atoms are bound to each of the phenyl groups in an η^2 (Cu2) or η^3 (Cu3) fashion.

A structurally different 1:2 adduct, **11b**, was obtained from a solution containing **3** and a large excess of AgOTf. XRD analysis of **11b** (Figure 5) revealed the presence of one-dimensional chains consisting of Ag−**3**−Ag units connected by a triflate anion, the Ag_2Pt plane being a crystallographic symmetry plane. Both triflate anions in the structure are disordered and have been refined on two positions, which precludes an accurate estimation of the corresponding bonding parameters. The Ag1 atom is bound to the platinum center *via* a short (2.7616(8) Å), unsupported Pt→Ag bond which makes an angle of 86° with the ligand plane, and is thus very similar to the Pt→Cu bond found in structure **4b**. The coordination of the Ag1 cation is completed by two oxygen atoms from different triflate anions and is roughly trigonal planar. The Ag2 atom is bound to **3** in a fashion similar to the one found in **6a** and **7a**: the Pt−Ag2 distance of 3.1694(9) indicates at most a weak d^8-d^{10} interaction, and the bonding mainly consists of Ag(I)−Phenyl contacts. The small difference between the Ag2−C1 and Ag2−C2 contacts (2.500(6) and 2.638(8) Å) entices us to describe these interactions as a distorted η^2 coordination, in contrast with the η^1 mode found for the Cu−Phenyl bonds in **6a**. Another η^2 interaction with a benzene ligand and the bond to the bridging triflate anion complete the distorted tetrahedral coordination environment of Ag2.

In summary, XRD studies allowed us to identify two distinct binding modes of **2** and **3** to monovalent coinage metals. The first one, available for both **2** and **3**, consists of a single dative Pt→M bond, whose geometry is consistent with donation of electron density from the d_{z^2} of platinum(II) to the Lewis-acidic metal. The second mode, which is preferred for **3**, involves mainly coordination to the *ipso* carbon atoms of the platinum-bound phenyl groups, in an η^1 or η^2 fashion depending on the ionic radius of the coinage metal.

Solution-Phase Studies. The interaction of **2** and **3** with Cu(I) and Ag(I) was further characterized in solution by means of UV−vis and ^{1}H NMR spectroscopies.

The UV−vis spectrum of **2** in benzene (Figures 6 and 7, black line) exhibits one band at 416 nm and one band at 644 nm with two high-energy shoulders and one weak low-energy shoulder, in agreement with what was found by Scollard et al. [58] for a series of closely related compounds. Both bands exhibit a strongly negative solvatochromic effect of similar magnitude (see Supporting Information), indicating that the corresponding electronic excited states are less polar than the ground state. Following Scollard et al.,[58] we assign the lower energy band to a set of ^{1}(d(Pt)→π^*) singlet metal-to-ligand charge-transfer

(58) Scollard, J. D.; Day, M.; Labinger, J. A.; Bercaw, J. E. *Helv. Chim. Acta* **2001**, *84*, 3247–3268.

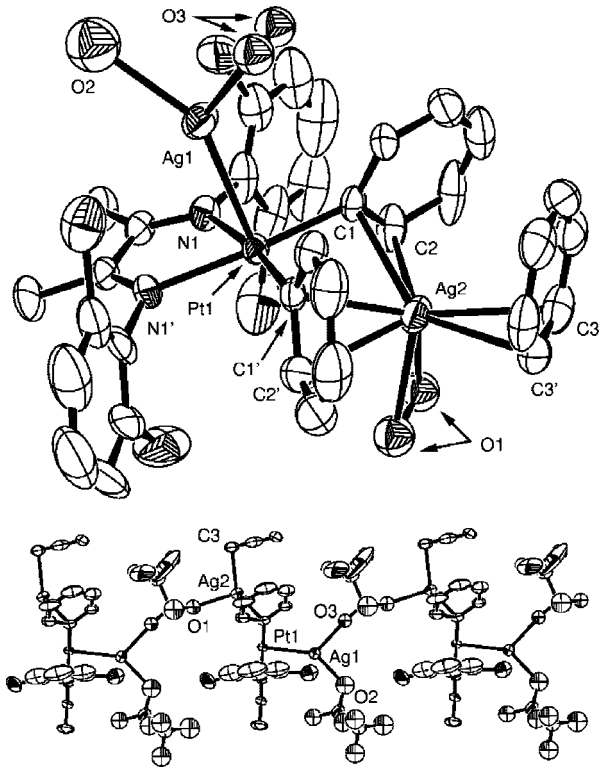

Figure 5. ORTEP representation of the X-ray crystal structure of **11b**. Ellipsoids are drawn at 50% probability. The $CF_3SO_3^-$ units are disordered and were refined isotropically over two symmetry-related positions with 50% occupancy each. Two unbound benzene molecules are omitted for clarity. Top: view of one $[PtAg_2]$ unit, including only the coordinated oxygen atoms of the disordered $CF_3SO_3^-$ units. Bottom: Side view of one one-dimensional chain. Selected distances [Å], angles [deg], and torsion angles [deg]: Pt1−Ag1 2.7616(8), Pt1−Ag 2 3.1694(9), Pt1−C1 2.009(7), Pt−N1 2.104(6), C1−Ag2 2.500(6), C2−Ag2 2.638(8), C3−Ag2 2.534(8), Ag1−Pt−Ag2 122.30(3), C1−Pt1−Ag1 93.18(18), N1−Pt1−Ag1 87.20(14), C1−Pt1−C1′ 92.0(4), C1−Pt1−N1 96.7(3), N1−Pt1−N1′ 74.6(3), Pt1−C1−Ag 2 88.6(2), C1−Ag1−C1′ 70.6(3), C1−Pt1−C1′−C2′ 113.6(6).

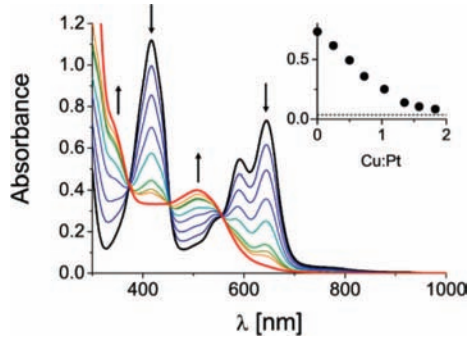

Figure 6. UV−vis absorption of 1.96×10^{-4} M solutions of **2** in benzene containing 0 −1.83 equiv of CuOTf. The black spectrum corresponds to pure **2** and the red one to **2** in the presence of a large excess of CuOTf. (Inset) Absorbance at 644 nm as a function of the Cu:Pt ratio. The dashed line corresponds to the absorbance in the presence of excess CuOTf.

(^{1}MLCT) transitions. However, these authors' assignment of the higher energy band to a $^1(\pi\rightarrow\pi^*)$ ligand-centered (^{1}LL) transition seems questionable in the case of complex **2** because of the important solvent sensitivity of this band. Thus, we propose that the band is at least partially due to $^1(d(Pt)\rightarrow\pi_2^*)$ MLCT transitions.

The UV−vis spectra of benzene solutions containing ~2×10^{-4} M of the dimethylplatinum(II) complex **2** and various amounts of CuOTf·$1/2C_7H_8$ are plotted in Figure 6. The bands at 644 and 416 nm are progressively depleted upon addition of CuOTf·$1/2C_7H_8$, and a band at 507 nm simultaneously appears. A band at ~350 nm also appears as a shoulder of the growing band at ~320 nm, which is due to a $^1(d(Cu)\rightarrow\pi^*(benzene))$ MLCT transition of free CuOTf·$1/2C_6H_6$.[59] The presence of three clean isosbestic points indicates that a single equilibrium is involved, which we attribute to the formation of the crystallographically characterized 1:1 adduct **4a** (Scheme 3). The blue shift of the ^{1}MLCT bands is consistent with the description of the Pt−Cu bond as a donor−acceptor bond, the platinum d_{z^2} orbital being stabilized by its interaction with the Cu(I) cation. However, the considerable modification of the fine structure of the first band makes it difficult to accurately quantify the energy shift.

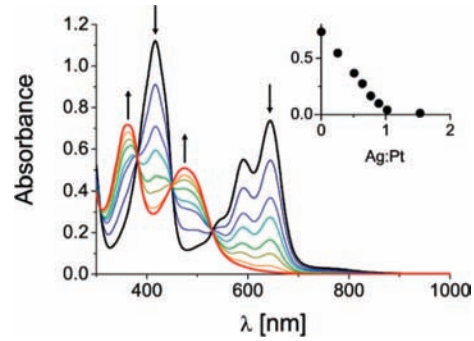

Figure 7. UV−vis absorption of 1.97×10^{-4} M solutions of **2** in benzene containing 0 (black) to 1.53 (red) equiv of AgOTf. (Inset) Absorbance at 644 nm as a function of the Ag:Pt ratio.

The behavior of **2** in the presence of silver(I) triflate is similar, as seen in the UV−vis titration data plotted in Figure 7. The first ^{1}MLCT band (λ_{max} = 644 nm in **2**) undergoes a more pronounced blue shift upon coordination to Ag(I) (λ_{max} = 475 nm) compared to Cu(I) (λ_{max} = 507 nm). As in the case of CuOTf, the observation of clean isosbestic points establishes the formation of a single complex in solution, which is assigned to the monomeric species **5a** (Scheme 3) on the basis of pulsed magnetic field gradient NMR (PFG-NMR) diffusion measurements (*vide infra*). The lack of knowledge of the aggregation state of CuOTf and AgOTf in benzene solution precludes the establishment of appropriate equilibrium equations, and thus no quantitative determination of association constants was attempted. However, the comparison of the traces obtained at λ = 644 nm for both coinage metals qualitatively shows that the association constant is higher for **5a** than for **4a**.

The electronic consequences of the formation of Pt→M bonds were also investigated by ^{1}H NMR spectroscopy. Since the UV−vis data show that there is only one adduct involved in both cases, the ^{1}H NMR spectra of **4a** and **5a** (Figure 8) were recorded in the presence of an excess of the corresponding triflate to ensure the absence of uncomplexed **2**. The resonance corresponding to the methyl groups of the α-diimine ligand shifts downfield by 0.76 and 0.77 ppm upon complexation to CuOTf and AgOTf, respectively. This shift most likely originates from inductive effects, the electron density depletion on the Pt(II) center translating into a net deshielding of the methyl protons. The effect of complexation on the platinum-bound methyl ^{1}H resonances seems to be more complex, since they are shifted by only a small amount and toward higher field.

(59) Kunkely, H.; Vogler, A. *Chem. Phys. Lett.* **2003**, *368*, 49–52.

Scheme 3[a]

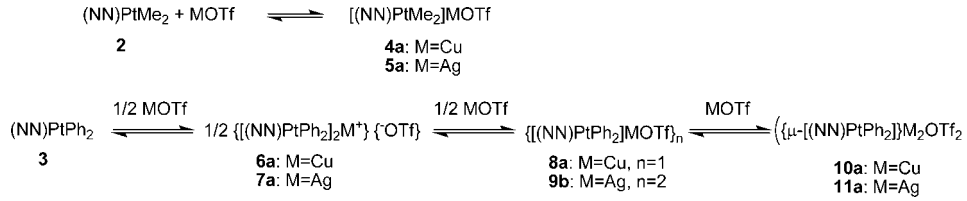

[a] Evidence for the existence of the 2:1 complexes **10a** is found by ^{1}H NMR at ~2.5 × 10^{-2} M, but not at concentrations relevant for UV−vis spectroscopy (~2 × 10^{-4} M). No evidence for the formation of **11a** in solution was found.

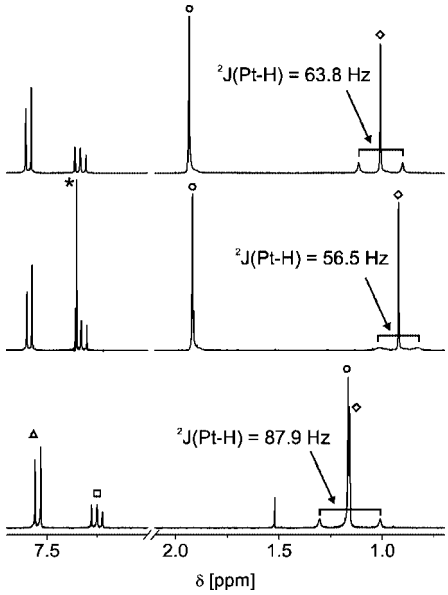

Figure 8. ^{1}H NMR spectra of **2** pure (bottom), and in the presence of an excess CuOTf (middle) or AgOTf (top). Peak assignment: $NAr^{3,5}$, Δ; NAr^4, □; C*Me*, ○ Pt*Me*, ◇. The peak of benzene coming from CuOTf·1/2C_6H_6 is marked with *.

Table 1. Diffusion Coefficients (*D*) and Hydrodynamic Volumes (V_H) Measured by PFG NMR.

sample	D (× 10^{-10} m^2 s^{-1})	V_H (nm^3)
2	13.4	0.41
2+CuOTf[a] (**4a**[b])	11.5	0.59
2+AgOTf[a] (**5a**[b])	12.7	0.47
3	12.7	0.47
6a	9.7	0.90
7a	9.5	0.94
3+CuOTf[a] (**8a**[b])	10.4	0.76
3+AgOTf[a] (**9b**[b])	8.7	1.19

[a] In equilibrium with solid MOTf. [b] Main species in solution.

The most striking effect on this signal is the substantial decrease of the $^2J(^{195}Pt-^1H)$ coupling constant from 87.9 Hz in **2** to 56.5 and 63.8 Hz in **4a** and **5a**, respectively.

The aggregation state of species **4a** and **5a** in solution was investigated by estimation of their hydrodynamic volume (V_H) using PFG NMR translational diffusion measurements (Table 1). Addition of an excess of CuOTf to a solution of **2a** in CD_2Cl_2 results in an increase of V_H from 0.41 to 0.59 nm^3, in accord with the formation of monomeric **4a**. The hydrodynamic volume obtained for **5a** (0.47 nm^3) is smaller than that of **4a**, showing that the solid-state dimer **5b** does not form in DCM solution. The difference between **4a** and **5a** may be due to partial dissociation of the Ag−OTf bond in solution.

The reaction of the diphenyl complex **3** with coinage metal triflates in solution is more complex than for **2**, as appears from

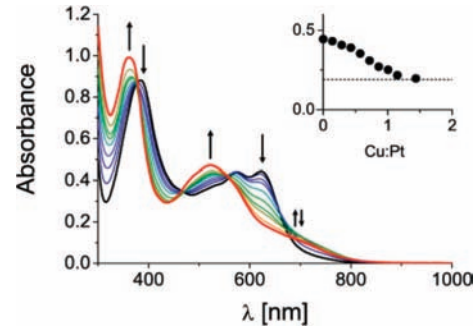

Figure 9. UV−vis absorption of 1.96 × 10^{-4} M solutions of **3** in benzene/dichloromethane 1:1 containing 0−1.43 equiv of CuOTf·1/2C_7H_8. The black spectrum corresponds to pure **3** and the red one to **3** in the presence of excess CuOTf·1/2C_7H_8. (Inset) Absorbance at 622 nm as a function of the Cu:Pt ratio. The dashed line corresponds to the absorbance in the presence of excess CuOTf·1/2C_7H_8.

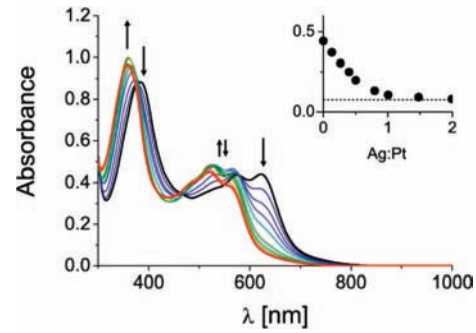

Figure 10. UV−vis absorption of 1.96 × 10^{-4} M solutions of **3** in benzene/dichloromethane 1:1 containing 0 (black) to 2.51 (red) equivalents of AgOTf. (Inset) Absorbance at 622 nm as a function of the Ag:Pt ratio. The dashed line corresponds to the absorbance in the presence of excess AgOTf.

the UV−vis titration data shown in Figures 9 and 10. This data was obtained in a 1:1 mixture of dichloromethane and benzene to avoid precipitation problems. The electronic spectrum of **3** resembles the one of **2**: a first band at 622 nm (646 nm in pure benzene) with two high energy shoulders, and a second, more intense band at 380 nm (387 nm in benzene) are observed. Both bands exhibit a strong negative solvatochromic effect (see Supporting Information). As for **2**, we assign the first band to a set of ^{1}(d(Pt)→π*) ^{1}MLCT transitions, and the second one to overlapping ^{1}LL and ^{1} MLCT transitions. Both bands undergo a blue shift upon addition of CuOTf or AgOTf, which likely originates from the stabilization of the HOMO *via* its interaction with the Lewis-acidic metal. Surprisingly, the addition of CuOTf to **3** also causes an increase in the absorbance between ~700 and 800 nm, resulting in a marked low energy shoulder on the first ^{1}MLCT band. Since this shoulder is not observed for the silver complexes, we tentatively assign it to a ^{1} (d(Cu)→π*) ^{1}MLCT transition, in accord with the higher stability of the Cu(II) oxidation state as compared to Ag(II).

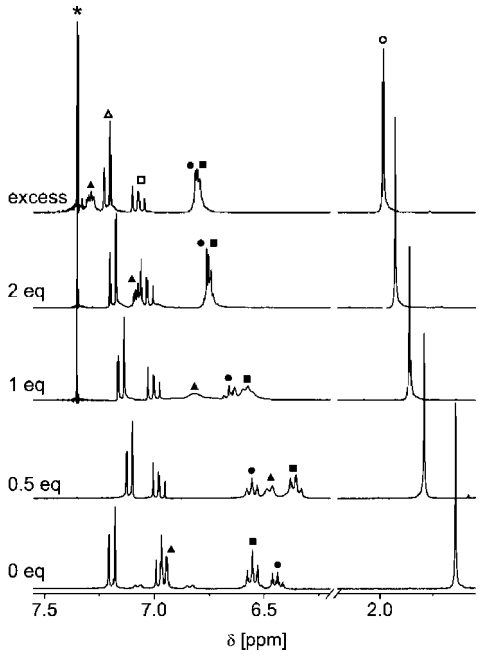

Figure 11. ^{1}H NMR spectra of ~25 mM solutions of **3** in CD_2Cl_2 containing various amounts of CuOTf. Peak assignment: $PtPh^{2,6}$, ▲; $PtPh^{3,5}$, ■; $PtPh^4$, ●; $NAr^{3,5}$, Δ; NAr^4, □; CMe, ○. The peak of benzene coming from CuOTf·$1/2C_6H_6$ is marked with *. It is absent in the spectrum with 0.5 equiv of CuOTf because the latter was recorded from crystallized **6a**.

In contrast to what is found for **2**, no isosbestic points are observed, and there are regions where the absorbance successively increases and decreases upon progressive addition of CuOTf·$1/2C_7H_8$ or AgOTf. This indicates that several equilibria are involved. The observation that, in both cases, the spectra do not evolve significantly for M:Pt (M = Cu, Ag) ratios above ca. 1.5, allows us to exclude the formation of complexes incorporating more than one MOTf unit per molecule of **3** in solution. Thus, we propose that the two leftmost equilibria depicted in Scheme 3 are taking place at these concentrations, involving the existence of both the crystallographically characterized 2:1 complexes **6/7a** and complexes with a M:Pt ratio of 1:1 (**8a** and **9b**, *vide infra*).

The existence of the two successive equilibria described in the previous paragraph was confirmed in the case of Cu(I) by recording ^{1}H NMR spectra of ca. 25 mM solutions of **3** in CD_2Cl_2 in the presence of various amounts of CuOTf·$1/2C_6H_6$ (Figure 11). Upon progressive addition of CuOTf, the resonances corresponding to the methyl groups (○) and the *para* hydrogen (●) atoms of the phenyl groups shift monotonically toward low field, which is easily explained by remote inductive effects. However, other peaks in the aromatic region of the spectrum follow a more complex trajectory. The most striking effect concerns the *ortho* hydrogen atoms of the phenyl groups (▲), whose resonance is easily identified by its double doublet (dd) structure and the satellite signals originating from ^{195}Pt−^{1}H coupling. This signal appears at δ 6.95 ppm for pure **3**. In the presence of 0.5 equivalent of CuOTf, this peak broadens and shifts toward high field to δ 6.47 ppm. At higher Cu:Pt ratios, it first becomes very broad and starts moving back to lower field, and is then found as a relatively sharp resonance at δ 7.08 ppm at a Pt:Cu ratio of 1:2, and finally at δ 7.30 ppm when the solution is saturated with CuOTf.

We rationalize these observations as follows: when only 0.5 equiv of CuOTf is present in solution, the major species is the 2:1 complex **6a**. As seen in the crystal structure of **6a** (Figure 3), the formation of the complex brings the phenyl groups of the two [(NN)$PtPh_2$] units in close proximity. Thus shielding of the *ortho* protons of the phenyl groups by phenyl groups of the second [(NN)$PtPh_2$] moiety accounts for the shift of the corresponding peak toward high field. When more CuOTf·$1/2C_6H_6$ is added, the concentration of the 1:1 adduct **8a** increases, and purely inductive effects cause the downfield shift of the whole spectrum. The substantial downfield shifts observed from the spectrum with two equivalents to that with a large excess of CuOTf·$1/2C_6H_6$ may indicate the formation of a small amount of the 1:2 adduct **10a** (Scheme 3). This contrast with the UV−vis spectroscopic observations is supposedly due to the higher concentration (2.5×10^{-2} vs 2×10^{-4} M) and solvent polarity (pure dichloromethane vs 1:1 benzene/dichloromethane). The ^{1}H NMR resonances of **3** also shift upon addition of AgOTf, but strong overlap in the aromatic region precludes a detailed interpretation of the obtained spectra (see Supporting Information). However, we observed that the ^{1}H NMR spectra of **3** in the presence of 1 equiv or an excess of AgOTf are identical, showing that the 1:2 adduct **11a** is not formed in dichloromethane solution.

More information about the solution-phase structure of the adducts of **3** with CuOTf and AgOTf is gained by PFG NMR experiments (Table 1). The hydrodynamic volume of **6a** (0.90 nm^3) and **7a** (0.94 nm^3) are almost identical and about twice as large as that of **3** (0.47 nm^3), in accord with their formulation as isostructural 2:1 adducts. When an excess of CuOTf is added to a solution of **6a**, the measured hydrodynamic volume decreases to 0.76 nm^3, indicating the formation of the smaller, mononuclear 1:1 complex **8a** and ruling out the existence of high-nuclearity clusters like **12** in solution. In contrast, addition of AgOTf to a solution of **7a** results in an increase of V_H to 1.19 nm^3, which strongly suggests that the main species is the 2:2 adduct **9b** (Scheme 3). The detailed structure of **9b** is unknown.

UV−vis and ^{1}H NMR data consistently show that the Pt→M bonds observed in the solid-state structures **4a** and **5b** also exist in solution. With complex **3** as the ligand, the 2:1 complexes **6a** and **7a**, the 1:1 complexes **8a**, and the 2:2 complex **9b** are formed, and evidence for the existence of the 1:2 adducts of CuOTf **10a** is found at high overall concentrations. Coordination of **2** and **3** to Cu(I) and Ag(I) results in a blue shift of absorption bands corresponding to ^{1}MLCT transitions in all cases. This observation parallels the one by Forniés et al.[28] of a similar blue shift of the MLCT band of the $[Pt(bzq)(C_6F_5)_2]^-$ (bzq = 7,8-benzoquinolate) anion upon coordination to the $(Ph_3P)Ag^+$ cationic fragment through a Pt→Ag dative bond. The interaction of the platinum complexes **2** and **3** with coinage metal triflates generally results in a shift of most proton resonances toward low field in the ^{1}H NMR spectrum, which is most likely due to inductive effects. Additionally, in the case of the dimethyl complex **2**, a substantial decrease of the $^2J(^{195}Pt-H)$ coupling constant upon complexation is observed. Similar reductions of the $^2J(^{195}Pt-H)$ coupling constant in the [(bpy)$PtMe_2$] complex from 86 to 64 Hz and 75 Hz upon coordination to the $(Ph_3P)Au^+$ and $(Ph_3P)Ag^+$ fragments, respectively, were observed by Puddephatt.[34] This effect thus appears to be diagnostic for the presence of Pt→M bonds in solution.

Gas-Phase Study. The interaction of **2** and **3** with coinage metal monocations was also studied in the gas phase by means of electrospray ionization mass spectrometry (ESI-MS). Electrospraying dilute acetonitrile solutions containing either **2** or

Scheme 4[a]

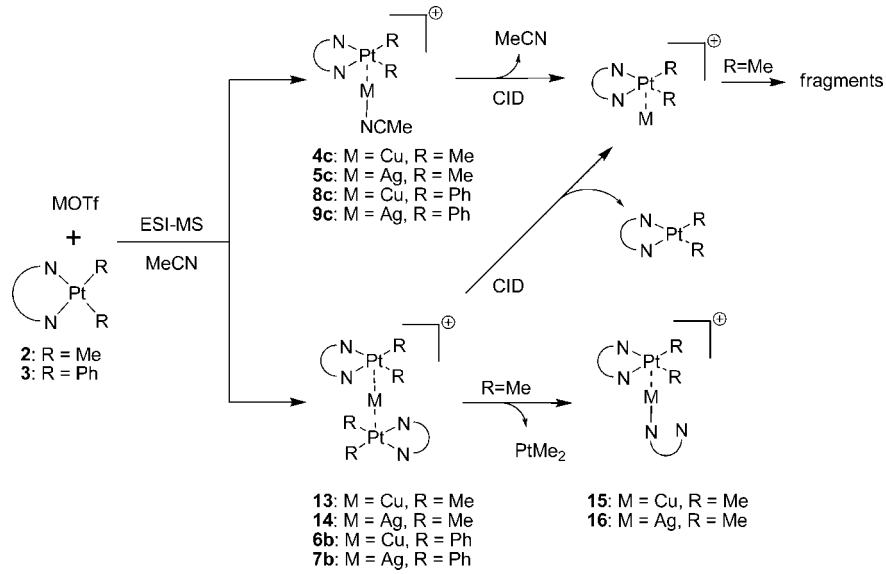

[a] Dashed bonds represent Pt→M dative bonds for R = Me and the interaction of M with the π electrons of phenyl groups for R = Ph (see Figure 13).

Table 2. CID Fragmentation Patterns for Cations **4c**, **5c**, **8c**, **9c**, **13**, **14**, **6b**, **7b**

ion	*m/z*	CID fragments
4c	704	663 (−MeCN), 681 (−MeCN + H_2O), 645 (−MeCN − CH_4), 547 (−MeCN − CH_4 − CuCl[a]), 437 (−MeCN − $PtMe_2$)
13	1261	1035 (−$PtMe_2$), 663 (−(NN)$PtMe_2$), 645 (−(NN)$PtMe_2$ − CH_4), 547 (−(NN)$PtMe_2$ − CH_4 − CuCl[a]), 437 (−(NN)$PtMe_2$ − $PtMe_2$)
5c	748	707 (−MeCN), 481 (−MeCN − $PtMe_2$)
14	1308	1081 (w, −$PtMe_2$), 707 (−(NN)$PtMe_2$), 481 (w, −(NN)$PtMe_2$ − $PtMe_2$)
8c	828	787 (−MeCN)
6b	1510	787 (−(NN)$PtPh_2$)
9c	872	831 (−MeCN)
7b	1554	831 (−(NN)$PtPh_2$)

[a] Formed by activation of a C−Cl bond of the diimine ligand.

3 and CuOTf or AgOTf allowed the clean observation of solvated 1:1 complexes which we presume have the structures **4c**, **5c**, **8c**, and **9c** (Scheme 4). Additionally, weaker signals corresponding to the 2:1 complexes **13**, **14**, **6b**, and **7b** also appeared in the corresponding spectra. Collision induced dissociation (CID) spectra were recorded for each individual ion, and the resulting fragments are listed in Table 2.

The main dissociation pathway for the 1:1 cations **4c**, **5c**, **8c** and **9c** is the loss of the coordinated acetonitrile, followed by further fragmentation in the case of **4c** (Figure 12). While this may appear unsurprising, it gives some information about the strength of the Pt→M bonds, showing that they are in all cases stronger than the MeCN−M coordination bonds. For comparison, the gas-phase dissociation energy of an acetonitrile ligand from the linear $[(MeCN)_2M]^+$ cations have been experimentally determined as 57.0 kcal/mol for M = Cu[60] and 34.6 kcal/mol for M = Ag.[61]

When **3** is the ligand, the 2:1 complexes **6b** and **7b** cleanly lose one [(NN)$PtPh_2$] unit upon CID. In contrast, the fragmentation of the 2:1 complexes **13** and **14** is more complex (Figure 12, Table 2). In addition to the expected loss of the [(NN)$PtMe_2$] fragment **2** and subsequent fragmentation, cations **13** and **14** can also lose a naked $PtMe_2$ neutral fragment; for the Cu(I) containing cation **13**, this is even the main CID channel (Figure 12). The structures of the cationic fragments cannot be unambiguously determined, but the simplest possible structures would be **15** and **16** (Scheme 4), in which one Pt→M bond is conserved and the second α-diimine ligand is coordinated to the coinage metal M. While this process in itself is of limited interest, its observation shows that d^8−d^{10} bonds can be strong enough to support ligand scrambling processes between two metals in the gas phase. This suggests that, with the right ligand

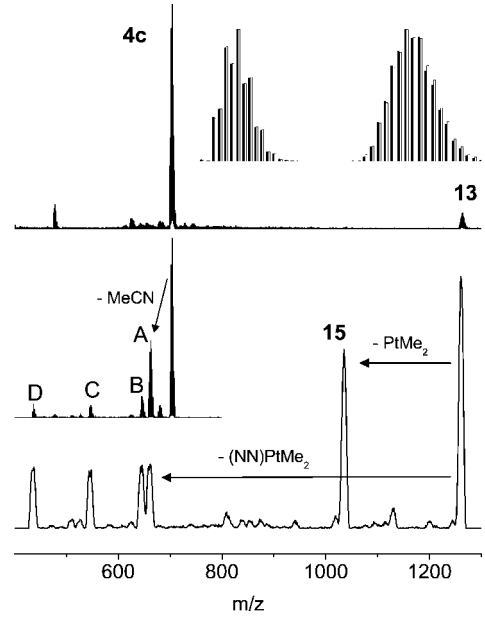

Figure 12. Top: ESI-MS spectrum of a solution of **2** and CuOTf in MeCN; experimental (black) and calculated (white) isotope patterns. Middle: CID spectrum of **4c**. Bottom: CID spectrum of **13**. Peak assignment: A: $\{[(NN)PtMe_2]Cu\}^+$, B: A − CH_4, C: B − CuCl, D: $[(NN)Cu]^+$.

(60) Vitale, G.; Valina, A. B.; Huang, H.; Amunugama, R.; Rodgers, M. T. *J. Phys. Chem. A* **2001**, *105*, 11351–11364.
(61) Shoeib, T.; El aribi, H.; Siu, K. W. M.; Hopkinson, A. C. *J. Phys. Chem. A* **2001**, *105*, 710–719.

Table 3. Comparison between Experimental (XRD) and Calculated (BP86/6-31+G(d);Cu,Ag,Pt:SDD) Values for Selected Distances (Å)

	4a		5b		6a	
	exp	calc	exp	calc	exp	calc
Pt−M[a]	2.399	2.438	2.829	2.917	2.725	2.758
			2.910	2.930		
M−O[a]	1.907	1.888	2.354	2.328	−	−
M−C[a,b]	2.929	3.131	2.829	2.915	2.138	2.164
	3.003	3.135	2.970	2.959	2.336	2.361
Pt−C	2.032	2.050	2.039	2.057	2.022	2.046
	2.039	2.050	2.043	2.057	2.033	2.061
Pt−N	2.110	2.176	2.117	2.181	2.082	2.152
	2.100	2.175	2.118	2.183	2.106	2.164

[a] M = Cu for **4a** and **6a**, M = Ag for **5b**. [b] No chemical bond for **4a** and **5b**.

combination, a process of fundamental interest like transmetalation could be studied on related complex ions.

DFT Calculations. The various experimental investigations described in the previous sections were complemented by theoretical studies using density functional theory. These calculations were performed with two main goals. The first one was to clarify the structure of compounds whose existence was implied by solution phase data but for which no XRD structure could be obtained, namely the 1:1 adduct **8a** and its silver analogue **9a**. The second objective was to get a more precise description of the bonding in the various compounds described in this work.

The geometries of the 1:1 adducts **4a**, **5a**, **8a**, and **9a**, as well as the dimeric structure **5b** and the 2:1 cations of **6b** and **7b**, were optimized at the BP86 level with a Pople-type 6-31+G(d) basis set on main group elements and the Stuttgart-Dresden[62,63] effective core potentials and basis sets on transition metals. The overall geometries of compounds characterized by XRD are well reproduced by our calculations. The comparison between selected experimental and calculated bond lengths (Table 3) shows that DFT tends to slightly overestimate the metal−ligand and metal−metal bond lengths, but calculated values are always within 4% of the experimental ones. The ability of this DFT method to predict the length of the unsupported Pt→M bonds in **4a** and **5b** is remarkable given its generally poor treatment of dispersion forces.[1] While error cancelation may be partially responsible for the good performance of DFT, we tentatively attribute it to the strong donor−acceptor character of these Pt→M bonds as compared to usual van der Waals or metallophilic bonds.

For the 1:1 adduct **8a** we found two structures involving two different coordination modes of the [(NN)$PtPh_2$] moiety (Figure 13). In the first one, labeled **8a1**, the Cu(I) cation makes a relatively short (2.668 Å) bond with the Pt(II) center, and is coordinated in an η^2 fashion to only one of the phenyl groups. The coordination to Cu(I) induces a lengthening of the corresponding Pt−C bond (2.048 vs 2.022 Å) and a distortion of the square planar geometry around the platinum center: the Pt−C bond makes an angle of 16° with the plane containing the three other ligands. While not optimal, the angle of 64° between the Pt−Cu axis and the ligand plane should allow for a significant donation of the d_{z^2} of the Pt(II) center to the Cu(I) atom. Interestingly, this binding mode is very similar to the one found in the more complex tetranuclear structures of type [(baimp)$PtPh_2$]$_2Cu_2$ (baimp = 3,5-bis(4-aryliminoacetyl)-4-methylpyrazolate).[37]

In the second structure, labeled **8a2**, the binding mode is the one a found in the 2:1 complex **6a** and in the 2:6 adduct **12**: the copper atom has close contacts (2.098 and 2.128 Å) with the *ipso* carbon atoms of both phenyl ligands, and the Pt−Cu axis makes an angle of 27° with the plane of the ligands around the platinum atom. The Pt−Cu distance (2.654 Å), however, is remarkably short, and should allow for a significant metal−metal interaction. The longer Pt−Cu bond length (2.758 Å) calculated for the 2:1 cation of **6a** is likely due to steric repulsion between the two [(NN)$PtPh_2$] moieties.

Two similar isomers are found for the silver complex **9a**. However, some noticeable differences are found between structures **9a2** and **8a2**. The silver atom in **9a2** has a short contact to only one of the phenyl *ipso* carbon atoms (2.321 vs 2.640 Å), but it is also close to one of the *ortho* carbon atoms (2.566 Å). Thus, the Ag(I) center in **9a2** is coordinated by a single phenyl group in a distorted η^2 fashion, while the Cu(I) center in **8a2** experiences η^1 coordination from both phenyl groups in an almost symmetrical way. Another difference is the fact that the Ag−Pt distance in **9a2** (3.059 Å) is significantly larger than that in **9a1** (2.847 Å), reflecting a relatively weak metal−metal interaction.

The difference between copper(I) and silver(I) is also apparent in the computed relative energies of the two isomers (Figure 13): structure **8a2** is predicted to be more stable than **8a1**, while **9a2** is higher in energy than **9a1**. The simplest explanation to these observations is based on the different ionic radii of Ag(I) and Cu(I). The smaller Cu(I) cation fits well in the cavity formed by the two phenyl ligands and the Pt(II) center, and it is able to maximize its interactions with these three groups in structure **8a2**. On the other hand, the Ag(I) cation is too voluminous for this cavity and preferentially binds to only one phenyl group in an η^2 fashion and to the platinum center, which is most efficiently achieved in structure **9a1**.The binding mode found in **9a1** leaves more accessible space around the silver(I) ion, which may explain the observation of the dimer **9b** in solution.

Some insight into the nature of the interaction of the organometallic platinum complexes **2** and **3** with Lewis-acidic metals is gained by considering their computed Kohn−Sham (KS) orbital structures (Figure 14). In compound **2**, the highest occupied molecular orbital (HOMO) is the d_{z^2} orbital of the platinum atom, as expected for a square planar d^8 transition metal complex. The lowest unoccupied molecular orbital (LUMO) is a π^* orbital of the α-diimine ligand, which is consistent with the assignment of the first band in its UV−vis spectrum to ^{1}(d(Pt)→π^*) ^{1}MLCT transitions (*vide supra*). The situation is slightly different for the diphenyl complex **3**. In this case, there is an important interaction between the filled π orbitals of the phenyl ligands and the d_{xy} orbital of the metal. As a result, the HOMO is an antibonding combination of these orbitals, and the d_{z^2} orbital is found at the HOMO−1 level.

The mapping of the electric potential (MEP) at the surface of molecules **2** and **3** is also represented in Figure 14. In accord with the KS orbital structure, compound **2** exhibits a single zone of strongly negative potential above the Pt(II) center. For compound **3**, the most negative region is found in between the two phenyl groups, but the space above the platinum atom also experiences a distinctly negative potential. Comparison with the experimental (XRD) and calculated structures of the MOTf adducts (M = Ag, Cu) shows that the MEP strongly correlates

(62) Bergner, A.; Dolg, M.; Kuechle, W.; Stoll, H.; Preuss, H. *Mol. Phys.* **1993**, *80*, 1431.
(63) Dolg, M.; Stoll, H.; Preuss, H.; Pitzer, R. M. *J. Phys. Chem.* **1993**, *97*, 5852.

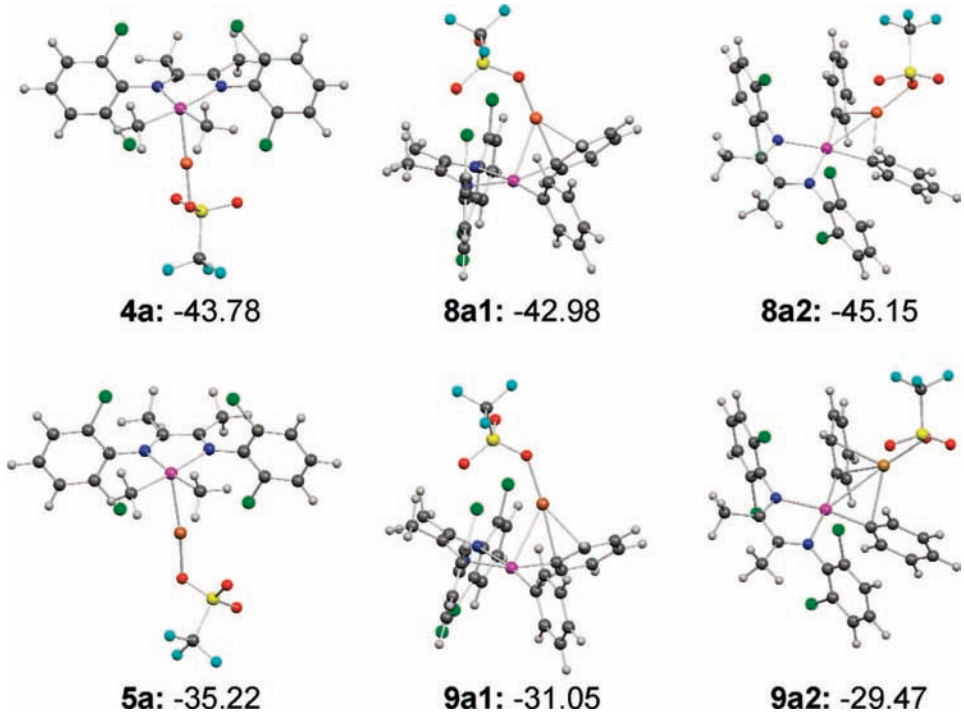

Figure 13. Calculated structures (BP86/6-21+G(d);Cu,Pt,Ag:SDD) and binding energies (BP86/TZ2P) [kcal/mol] for the 1:1 adducts **4a**, **5a**, **8a**, and **9a**. Colors: H light gray, C dark gray, N dark blue, O red, F light blue, S yellow, Cl green, Cu orange, Ag brown, Pt purple. Selected bond lengths [Å] (in cases where the two C (N) atoms are not equivalent, the value corresponding to the atom which is closest to the coinage metal is marked with *): **4a**: Pt−Cu 2.438; Pt−C 2.050, 2.050; Pt−N 2.175, 2.176; Cu−O 1.888. **5a**: Pt−Ag 2.661; Pt−C 2.050, 2.050; Pt−N 2.170, 2.175; Ag−O 2.199. **8a1**: Pt−Cu 2.668; Pt−C 2.048*, 2.022; Pt−N 2.198*, 2.138; Cu−O 1.918; Cu−C^{ipso} 2.115; Cu−C^{ortho} 2.155. **8a2**: Pt−Cu 2.654; Pt−C 2.059*, 2.062; Pt−N 2.139*, 2.141; Cu−O 1.987; Cu−C^{ipso} 2.098*, 2.128; Cu−C^{ortho} 2.466*, 2.574. **9a1**: Pt−Ag 2.847; Pt−C 2.036*, 2.022; Pt−N 2.203*, 2.149; Ag−O 2.185; Ag−C^{ipso} 2.516; Ag−C^{ortho} 2.434. **9a2**: Pt−Ag 3.059; Pt−C 2.048*, 2.041; Pt−N 2.161*, 2.137; Ag−O 2.228; Ag−C^{ipso} 2.321*, 2.640; Ag−C^{ortho} 2.566*, 2.709.

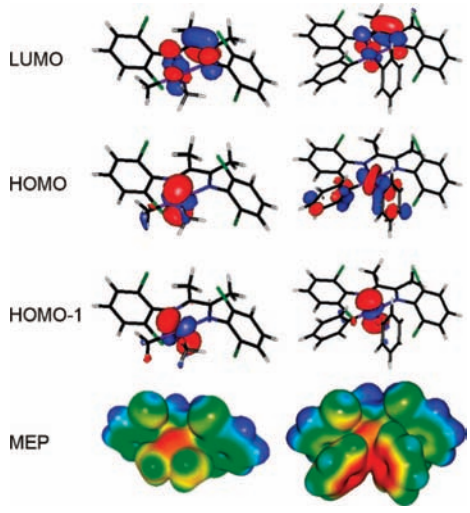

Figure 14. Frontier Kohn−Sham orbitals and mapping of the electric potential (MEP) from −0.055 (red) to +0.055 (blue), projected on an isodensity surface for compounds **2** (left) and **3** (right)

with the observed binding modes. In all complexes of the dimethyl complex **2** the coinage metal is found right on top of the square planar Pt(II) center, while in most complexes of the diphenyl complex **3** η^1 or η^2 coordination of the phenyl groups is preferred. The 1:2 adduct **11b** offers an example of a structure where both positions are occupied. Thus, a simple electrostatic model is able to predict the locations of the Cu(I) and Ag(I) metals in the corresponding adducts, which suggests that these interactions are mainly electrostatic in nature, the coinage metal cation acting like a "fat proton".

Therefore, structures **4a** and **5a** can be seen as isolobal analogues of the pentacoordinate Pt(IV) hydride complexes that are thought to be intermediates in the protolysis of Pt(II) dialkyl[41,64] and diaryl[39,41,65] complexes. On the other hand, **8a** and **9a** resemble more the transition state for the reductive elimination of benzene from the Pt(IV) intermediate. This difference between d^{10} metal cations and H^+ can be understood from the fact that the former are softer Lewis acids, allowing for a stronger interaction with the π electrons of the phenyl rings.

A semiquantitative estimation of the different contributions to the computed bond dissociation energies (BDEs) was obtained by performing an energy partitioning analysis[66] on the computed structures for the 1:1 adducts **4a**, **5a**, **8a** and **9a**. The total binding energy ΔE of the [(NN)PtR_2] and MOTf fragments is decomposed into the preparation energy, ΔE_{prep}, and the interaction energy, ΔE_{int}. ΔE_{prep} corresponds to the energy needed to deform the fragments from their optimal geometry to their geometry in the complex. ΔE_{int} is further split into the Pauli repulsion term, ΔE_{Pauli}, the electrostatic term, ΔE_{elstat}, and the orbital interaction term, ΔE_{orb}. Additionally, the extent to which charge transfer contributes to the binding was estimated by computing the Hirshfeld[89] charge on the [(NN)PtR_2] fragment in all complexes.

(64) Wik, B. J.; Ivanovic-Burmazovic, I.; Tilset, M.; van Eldik, R. *Inorg. Chem.* **2006**, *45*, 3613–3621.
(65) Ong, C. M.; Jennings, M. C.; Puddephatt, R. J. *Can. J. Chem.* **2003**, *81*, 1196–1205.
(66) Bickelhaupt, F.; Baerends, E. *Kohn-Sham Density Functional Theory: Predicting and Understanding Chemistry. In Rev. Comp. Chem.*, Vol. 15; Lipkowitz, K. B.; Boyd, D. B. , Eds.; Wiley-VCH: 2000.

Table 4. Energy Partitioning Analysis [kcal/mol] and Fragment Hirshfeld Charges for the Calculated Structures of **4a**, **5a**,**8a**, and **9a**

	4a	5a	8a1	8a2	9a1	9a2
ΔE_{Pauli}	57.05	45.27	103.38	129.97	75.81	80.10
ΔE_{elstat}	−62.18	−50.97	−94.9	−105.50	−73.78	−70.25
ΔE_{orb}	−43.89	−30.54	−64.28	−75.75	−45.92	−44.27
$\Delta E_{\text{int}}{}^{a}$	−49.02	−36.24	−55.82	−51.29	−43.90	−34.43
ΔE_{prep}	5.24	1.02	12.85	6.13	12.84	4.95
ΔE^{b}	−43.78	−35.22	−42.98	−45.15	−31.05	−29.47
$q((\text{NN})\text{PtR}_2)$	0.198	0.195	0.126	0.067	0.158	0.118

[a] $\Delta E_{\text{int}} = \Delta E_{\text{Pauli}} + \Delta E_{\text{elstat}} + \Delta E_{\text{orb}}$. [b] $\Delta E = \Delta E_{\text{int}} + \Delta E_{\text{prep}}$.

The contribution of orbital interaction to the sum of the attractive terms ranges from 37.5% for **5a** to 41.8% for **8a2**. Thus, the binding in all complexes is predominantly electrostatic, but orbital contributions are not negligible. It should be noted, however, that the term ΔE_{orb} also includes polarization effects, and thus the actual contribution of donor−acceptor orbital interaction is expected to be lower than ΔE_{orb}. The computed partition of the attractive terms is similar to what was found by Nechaev et al.[67] for simple ethylene and acetylene complexes of coinage metal cations, where the orbital interaction accounts for 40.6−44.2% of the attraction.

The computed charges of +0.198 and +0.195 on the [(NN)PtMe$_2$] fragments of **4a** and **5a** indicate an important charge transfer character of the d^8−d^{10} interactions in these compounds, in agreement with their description as Pt→M dative bonds. Structures **8a2** ($q((\text{NN})\text{PtPh}_2) = +0.067$) and **9a2** ($q((\text{NN})\text{PtPh}_2) = +0.118$) exhibit less charge transfer, which is probably compensated by the polarization of the π-electron density of the phenyl groups. An intermediate situation is found for structures **8a1** ($q((\text{NN})\text{PtPh}_2) = +0.126$) and **9a1** ($q((\text{NN})\text{PtPh}_2) = +0.158$), in which some interaction of the d_{z^2} orbital of Pt(II) with the coinage metal is expected due to its location above the plane of the ligands.

The two binding modes of the diphenyl complex **3** also differ by the magnitude of the preparation energy term, which is 2−3 times higher for **8a1** and **9a1** as for **8a2** and **9a2**. This difference is due to the out-of-plane bending of one of the Pt−C bonds that is required to maximize the interaction between the coinage metal and both the Pt(II) center and the phenyl ligand.

Another prominent feature of the data presented in Table 4 is the fact that Pt→M bonds are predicted to be significantly stronger for M = Cu(I) than for M = Ag(I). This may appear surprising in view of the small number of reported compounds incorporating Pt→Cu bonds, as compared to the large body of literature dealing with Pt→Ag bonds. These observations illustrate the fact that trends in the strength of a particular bond do not necessarily correlate with the overall stability of the corresponding compounds. In fact, compound **4a**, for example, is thermally less stable than **5a** in solution due to its easier disproportionation into Cu(0), Pt(II) and Pt(IV) products (*vide infra*).

C−H Activation Reactivity. In order to probe for the reactivity of compounds incorporating Pt→M bonds in relation with C−H bond activation, we studied the thermolysis of complexes **4a** and **5a** in benzene (Scheme 5). Heating a solution of **4a** prepared *in situ* in benzene for 3 days at 50 °C, followed by filtration over a short column of activated alumina, yielded 41% of the double C−H activation product **3** and 4% of free ligand **1**. The same treatment applied to the silver(I) complex **5a** afforded a slightly better yield of **3** (60%), and decomposition leading to free ligand **1** was less important (1%).

Scheme 5

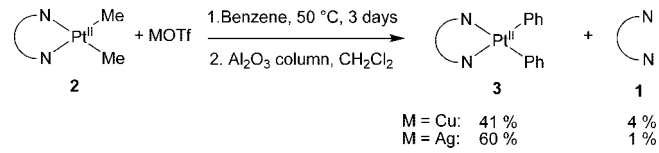

Monitoring these reactions *in situ* by ^{1}H NMR spectroscopy proved unfeasible due to the number of transient species and the formation of a range of MOTf adducts with different stoichiometry, but nevertheless allowed the detection of the produced methane as a mixture of isotopomers. Mechanistically relevant information could be obtained from ESI-MS analysis of samples of the reaction mixture diluted in acetonitrile. Figure 15 shows a spectrum obtained from a solution of **4a** in benzene after a reaction time of 17 h at 50 °C. This spectrum indicates the presence in the reaction mixture of starting material **2** and product **3**, as well as the half-reacted intermediate [(NN)Pt(Me)(Ph)] (**19**), observed as their solvated Cu^+ complexes. Additionally, the peaks at *m/z* 613 and 654 arise from the Pt(IV) fragment $[(\text{NN})\text{PtMe}_3]^+$, presumably formed by the facile dissociation of the triflate complex [(NN)PtMe$_3$(OTf)] (**17**). The peak at *m/z* 623 comes from the acetonitrile-solvated complex $[(\text{NN})\text{Pt(Me)(NCMe)}]^+$, which we attribute to the reaction of the weakly bound triflate complex [(NN)Pt(Me)(OTf)] (**18**) with acetonitrile. Finally, the presence of free ligand **1** is confirmed by the peak at *m/z* 478, which corresponds to its Cu(I) complex $[(\text{NN})\text{Cu(NCMe)}]^+$. Workup of this partially reacted mixture and analysis of the residue by ^{1}H NMR confirmed the presence of **1** (12%), **2** (27%), **19** (18%), and **3** (43%). The triflate-containing species **17** and **18** were not observed and were probably retained on the alumina column together with copper(I) triflate.

To check whether the activation of **2** toward C−H bond breaking could proceed through a reversible transfer of one methyl group to Cu(I) or Ag(I),[34] we conducted methyl scrambling experiments. A benzene solution containing approximately equal amounts of **2** and [(NN)Pt(CD$_3$)$_2$] (**2**-d$_6$), and an excess CuOTf, was stored at room temperature for 7 days. ESI-MS analysis (see Supporting Information) revealed the slow formation of the mixed species [(NN)Pt(CH$_3$)(CD$_3$)] (**2**-d$_3$), with concomitant C−H activation reaction leading to **3**. However, no methyl scrambling was observed under the same conditions with AgOTf, although the C−H activation reaction was found

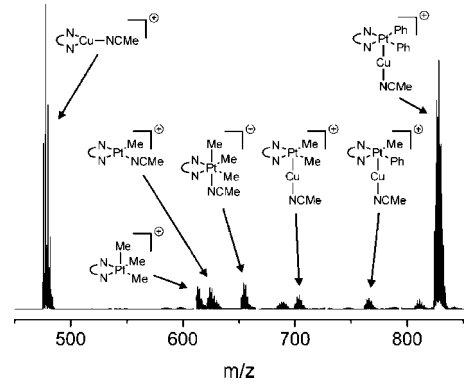

Figure 15. ESI-MS spectrum obtained from a reaction mixture containing **2** and one equivalent of CuOTf in benzene after 17 h at 50 °C, diluted in acetonitrile.

(67) Nechaev, M. S.; Rayon, V. M.; Frenking, G. *J. Phys. Chem. A* **2004**, *108*, 3134–3142.

Scheme 6

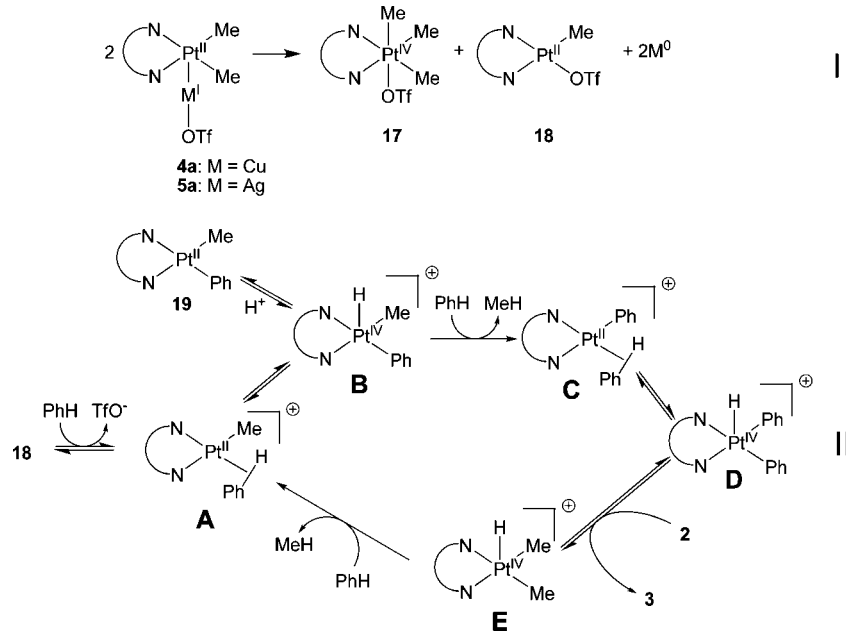

to proceed. Furthermore, the methyl-transfer pathway does not account for the appearance of Pt(IV) species in the ESI-MS spectra, and thus an alternative mechanism has to be involved.

We propose the mechanism presented in Scheme 6. The reaction is initiated by one-electron oxidation of the Pt(II) complex **2** by the coinage metal triflate (Scheme 6(I)), which leads to a postulated transient Pt(III) intermediate that disproportionates into the Pt(IV) complex **17** and the activated Pt(II) complex **18**. This initiation reaction consumes only a small fraction of the starting material. The next reaction is the actual double C−H activation of benzene promoted by species **18** (Scheme 6(II)). The labile triflate anion is exchanged for a benzene molecule to form the cationic intermediate **A**, which undergoes oxidative addition of the Ph−H bond to afford the Pt(IV) intermediate **B**. Reversible deprotonation of **B** accounts for the observation of the mixed complex **19**. Alternatively, **B** can undergo reductive elimination of methane followed by complexation of a second benzene molecule to produce intermediate **C**. A second oxidative addition step yields the Pt(IV) hydride complex **D**, which is able to transfer a proton to the starting material **2**, releasing the product **3**. Reductive elimination of methane and its displacement by a benzene molecule regenerates intermediate **A**, allowing for the production of several molecules of **3** for one molecule of **18** generated in the initiation step I. It should be noted that the proton transfer reaction **D** + **2** → **3** + **E** does not have to proceed in a single step, but may also involve protonation of the triflate anion by **D** to transiently form triflic acid, which would then protonate **2** to form intermediate **E**.

The one-electron oxidation chemistry proposed for the activation step (I) parallels that observed upon chemical or electrochemical oxidation of closely related complexes in acetonitrile.[58,68,69] Furthermore, a related process has been observed in the reaction of [(bpy)$PtMe_2$] with CuCl, yielding [(bpy)$PtMe_3Cl$], [(bpy)PtMeCl] and Cu(0).[34] The availability of this pathway for **2** was shown by oxidizing **2** with one equivalent of ferrocenium triflate in acetone-d_6, affording equimolar amounts of **17** and **18**. The assignment of the products was made by comparison of the ^{1}H NMR spectrum with that of independently synthesized **17** and that of **18** generated *in situ* from [(NN)PtMeCl] (**20**) and AgOTf. To prove that one-electron oxidation chemistry is sufficient to explain the observed double C−H activation reaction, we heated a benzene solution containing compound **2** and 10 mol% of ferrocenium triflate to 50 °C for 3 days. ^{1}H NMR analysis of the reaction mixture revealed that nearly quantitative formation of the diphenyl complex **3** had occurred. Additionally, reduced ferrocene and a small amount of the Pt(IV) trimethyl complex **17** were observed, indicating that the latter is not responsible for the C−H activation chemistry.

The methyl scrambling observed for the copper(I) complex **4a** can be explained by the formation of trace amounts of the Pt(IV) complex **17** *via* the redox reaction depicted in Scheme 6(I). Despite its low solubility in benzene, compound **17** was found to be able to transfer methyl groups to **2**-d_6, presumably *via* an S_N2-type reaction of the nucleophilic Pt(II) center of **2** and an electrophilic methyl group of **17**[70,71] (Scheme 7). This reaction is expected to proceed only for the free complex **2** in equilibrium with **4a**, since complexation to a Lewis-acidic metal should strongly decrease the nucleophilicity of the Pt(II) center. The fact that no methyl scrambling is observed for the silver complex **5a** is thus attributed to its stronger association constant (*vide supra*).

Related double C−H activation reactions have been observed for anionic complexes of type [(LL)$PtMe_2$]$^-$ (LL = dimethylbis(2-pyridyl)borate,[72] diphenylbis(1-pyrazolyl)borate[73]), and for a homodinuclear Pt(II) complex.[74] The proposed mechanisms

(68) Wik, B. J.; Tilset, M. *J. Organomet. Chem.* **2007**, *692*, 3223–3230.
(69) Johansson, L.; Ryan, O. B.; Rømming, C.; Tilset, M. *Organometallics* **1998**, *17*, 3957–3966.
(70) Aye, K. T.; Canty, A. J.; Crespo, M.; Puddephatt, R. J.; Scott, J. D.; Watson, A. A. *Organometallics* **1989**, *8*, 1518–1522.
(71) Hill, G. S.; Yap, G. P. A.; Puddephatt, R. J. *Organometallics* **1999**, *18*, 1408–1418.
(72) Khaskin, E.; Zavalij, P. Y.; Vedernikov, A. N. *J. Am. Chem. Soc.* **2006**, *128*, 13054–13055.
(73) Thomas, C. M.; Peters, J. C. *Organometallics* **2005**, *24*, 5858–5867.

Scheme 7

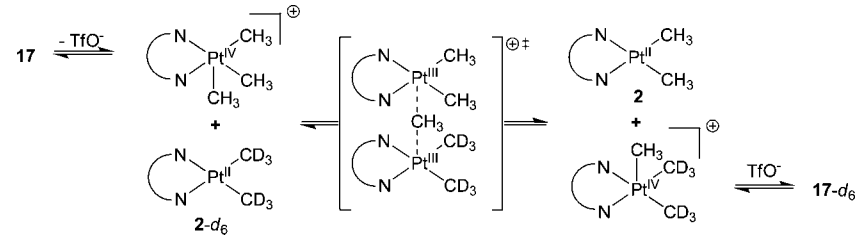

for these reactions parallel the one depicted in Scheme 6(II), the main difference being that the active Pt(II) methyl species is generated by protolysis[72−74] or methide abstraction[73] from the dimethyl complexes, whereas here it is produced by one-electron oxidation.

Conclusions

The electron-poor α-diimine ligand **1** was found to be efficient for the stabilization of structurally simple compounds formed by the interaction of organoplatinum(II) complexes with monovalent coinage metal triflates, without the need for an extra stabilizing or bridging ligand.

The dimethylplatinum complex **2** binds to the coinage metal through short, unsupported Pt→M bonds in the solid phase, in solution, and in the gas phase. The CuOTf adduct **4b** exhibits the shortest Pt−Cu contact known to date. DFT calculations shows that these interactions are essentially electrostatic in nature, but with a significant contribution from orbital interactions. In particular, a significant amount of charge transfer is computed, in accord with the observation of an important downfield shift of the ligand methyl ^{1}H NMR resonance and the blue shift of the ^{1}MLCT bands in the UV−vis absorbance spectra upon coordination. Thermolysis of the complexes in benzene produces the diphenyl complex **3** in moderate yield through a double C−H activation reaction. We propose that the mechanism of these reactions is similar to known double C−H activation processes,[72−74] except for the fact that in our case the active cationic Pt(II) species is generated through an oxidative process rather than protolysis or methide abstraction.

Electrostatic considerations based on DFT calculations predict a more complex binding situation for the diphenylplatinum complex **3**: the metal cation is able to bind either to the platinum center through a Pt→M bond or to the phenyl groups. In the solid state, we found that the latter is preferred in the homoleptic 2:1 complexes **6a** and **7a** as well as in the 2:6 complex **12**, while both binding sites are occupied in the 1:2 complex **11b**. Spectroscopic studies in solution revealed the existence of several complexes of **3** with coinage metal triflates, namely the 2:1 complexes **6a** and **7a**, the 1:1 complexe **8a**, the 2:2 complex **9b**, and possibly the 1:2 complex **10a** with copper(I) triflate at higher concentrations.

These results demonstrate the ability of simple organoplatinum compounds to act as ligands for Lewis-acidic metals. The physical properties of the platinum complexes change markedly upon coordination to monovalent coinage metal cations, and the Pt−M bonds have been found to be strong enough to support ligand exchange processes. Thus, we anticipate that complexes similar to the ones described in this study might allow for the observation of novel chemical processes based on d^8−d^{10} interactions. This is the subject of further investigations in our laboratories.

(74) Song, D.; Jia, W. L.; Wang, S. *Organometallics* **2004**, *23*, 1194–1196.

Experimental Section

General Procedures. Solvents were obtained commercially in p.a. quality and used as received. For reactions involving metal complexes, solvents were distilled under nitrogen over sodium (hexane, toluene), potassium (tetrahydrofuran, benzene), CaH_2 (acetonitrile, dichloromethane). All chemical manipulations involving metal complexes were performed under an inert atmosphere using standard Schlenk and glovebox techniques unless otherwise stated. Deuterated solvents were dried through a short column of activated alumina immediately before use. ^{1}H and ^{13}C chemical shifts are reported in ppm relative to tetramethylsilane, using residual solvent proton and ^{13}C resonances as internal standards. Multiplicities are indicated s (singlet), d (doublet), t (triplet), dd (double doublet), while apparent singlets, doublets and triplets are indicated by "s", "d", and "t", respectively. Elemental analyses were carried out at the Mikrolabor of the Laboratorium für Organische Chemie of ETH Zürich. Organolithium reagents were titrated using the procedure from Watson and Eastham.[75] Precursors *cis*-$PtPh_2(SMe_2)_2$[37] and *trans*-$(Me_2S)_2Pt(Me)Cl$,[76] α-diimine ligand **1**[54] and complex **2**[54] were prepared according to literature procedures. The diphenylplatinum(II) complex **3** was synthesized by a modification of the procedure by Gerdes.[56] All other chemicals were obtained commercially and used as received.

(NN)PtPh$_2$ (3). A mixture of **1** (897 mg, 1.89 mmol) and *cis*-$PtPh_2(SMe_2)_2$ (711 mg, 1.90 mmol) in toluene (20 mL) was stirred for 1 day. The solvent was then removed *in vacuo*, and toluene (20 mL) was added. This cycle was repeated three times, and the mixture was stirred for 3 days. Removal of the solvent *in vacuo*, washing of the residue with toluene (3 × 5 mL), and drying *in vacuo* yielded the product as a purplish-gray powder (1.21 g, 88%). **^{1}H NMR** (CD_2Cl_2, 300 MHz): δ 7.19 (d, ^3J(H−H) = 8.0 Hz, 4H, NAr*H*^{3,5}), 7.00−6.93 (m, 2H, NAr*H*^{4}), 6.95 (dd, ^3J(H−H) = 7.8 Hz, ^5J(H−H) = 2.2 Hz, ^3J(Pt−H) = 70.9 Hz, 4H, PtAr*H*^{2,6}), 6.61−6.49 (m, 4H, PtAr*H*^{3,5}), 6.44 (tt, ^3J(H−H) = 7.2 Hz, ^5J(H−H) = 1.4 Hz, 2H, PtAr*H*^{4}), 1.64 (s, 6H, C*H*$_3$). **Anal.**: calcd for $C_{28}H_{22}N_2Cl_4Pt$: C 46.49, H 3.07, N 3.87. Found: C 46.21, H 3.15, N 3.65.

[(NN)PtMe$_2$]CuOTf (4a). A mixture of **2** (50 mg, 83 μmol) and CuOTf·1/2C_7H_8 (24 mg, 93 μmol) in toluene (5 mL) was stirred for 30 min. A small amount of brown precipitate was removed by filtration, yielding a dark-red solution. Hexane (10 mL) was added, and the solution was stored at −20 °C for 7 days, during which time dark red needles formed. Solvent removal by decantation, washing with hexane (4 × 2 mL) and drying *in vacuo* yielded the product as dark, brownish-red needles (31 mg, 46%). **Anal.**: calcd for $C_{19}H_{18}N_2O_3F_3SCl_4CuPt$: C 28.11, H 2.23, N 3.45. Found: C 28.51, H 2.30, N 3.45. Crystals suitable for XRD were obtained at −35 °C from a freshly prepared solution of **4a** in 1:1 benzene/hexane; benzene precipitation initiated the crystallization, and the crystals that formed on the walls of the flask were mechanically separated from the solid benzene.

(75) Watson, S. C.; Eastham, J. F. *J. Organomet. Chem.* **1967**, *9*, 165–168.

(76) Hill, G. S.; Irwin, M. J.; Levy, C. J.; Rendina, L. M.; Puddephatt, R. J. *Inorg. Synth.* **1998**, *32*, 149–152.

$[(NN)PtMe_2]_2Ag_2(OTf)_2\cdot 2C_6H_6$ (5b·2C$_6$H$_6$). A mixture of **2** (60 mg, 0.1 mmol) and AgOTf (26 mg, 0.1 mmol) was stirred in benzene (7 mL) for 1 h, during which time a small amount of a dark-red precipitate appeared. The mixture was concentrated to 2 mL and filtered. Washing with benzene (3 × 1 mL) and drying *in vacuo* afforded the product as a purple powder containing two equivalents of benzene (60 mg, 64%). **Anal**: calcd for $C_{38}H_{36}N_4O_6F_6SCl_8Ag_2Pt_2\cdot 2C_6H_6$: C 32.14, H 2.59, N 3.00. Found: C 31.62, H 2.50, N 2.89. Crystals suitable for XRD were obtained from vapor diffusion of hexane into a benzene solution of **2** in the presence of a large excess of AgOTf. Solvated AgOTf crystallized as white needles at the same time.

$\{[(NN)PtPh_2]_2Cu\}^+TfO^-$ (6a). A mixture of **3** (100 mg, 0.138 mmol) and CuOTf·1/2C$_7$H$_8$ (20 mg, 0.077mmol) in dichloromethane (4 mL) was stirred for 10 min and filtered. Toluene (10 mL) was added to the resulting dark-purple solution, which was slowly concentrated under a flow of argon over 18 h. Filtration, washing with toluene (3 × 2 mL) and drying *in vacuo* yielded the **6a** as black needles suitable for XRD (60 mg, 52%). **Anal**: calcd for $C_{57}H_{44}N_4O_3F_3SCl_8CuPt_2$: C 41.26, H 2.67, N 3.38. Found: C 41.45, H 2.64, N 3.38.

$\{[(NN)PtPh_2]_2Ag\}^+TfO^-$ (7a). A mixture of **3** (50 mg, 69 μmol) and AgOTf (10 mg, 39 μmol) in dichloromethane (1.5 mL) was stirred for 2 min. Filtration and washing with dichloromethane (2 × 0.5 mL) yielded a deep-purple solution, to which toluene (4 mL) was added. Crystallization started after a few minutes, and the solution was kept at −20 °C overnight. Filtration, washing with toluene (3 × 1 mL), and drying *in vacuo* yielded the product as dark-purple plates (36 mg, 61%). **Anal**: calcd for $C_{57}H_{44}N_4O_3F_3SCl_8AgPt_2$: C 40.18, H 2.60, N 3.29. Found: C 40.28, H 2.72, N 3.40. Crystals suitable for XRD were obtained upon slow concentration of a solution of **7b** in THF/benzene or DCM/toluene.

$\{[(NN)PtPh_2]Ag_2(OTf)_2(C_6H_6)\}_n\cdot 2C_6H_6$ (11b·2C$_6$H$_6$). A solution of **3** (20 mg, 28 μmol) and AgOTf (20 mg, 78 μmol) in 1:1 dichloromethane/benzene was slowly concentrated under a flow of argon, resulting in the formation of red crystals suitable for XRD. Washing with hexane and drying *in vacuo* yielded the compound as a red solid (31 mg, 75%). The crystals lost about 0.5 equiv of benzene upon drying, as shown by elemental analysis. **Anal.**: calcd for $C_{36}H_{28}N_2O_6F_6S_2Cl_4Ag_2Pt\cdot 1.5C_6H_6$: C 37.73, H 2.60, N 1.96. Found: C 37.89, H 2.57, N 1.90.

$\{[(NN)PtPh_2]_2Cu_6(OTf)_6\}\cdot 6CD_2Cl_2$ (12·6CD$_2$Cl$_2$). A mixture of **3** (7 mg, 10 μmol) and CuOTf·1/2C$_6$H$_6$ (10 mg, 40 μmol) in CD$_2$Cl$_2$ (0.7 mL) was stirred for 5 min and the excess CuOTf·1/2C$_6$H$_6$ was removed by filtration, resulting in a dark-purple solution which was transferred into a Young-type NMR tube. The solution was left standing at 20 °C for 3 h and then cooled at 4 °C for 1 h, causing the crystallization a small amount of **12** as dark-purple needles which were suitable for XRD. No clean elemental analysis was obtained due to the concomitant formation of a grayish precipitate (presumably CuOTf) that could not be separated from **12**.

$(NN)Pt(Me)_3(CF_3SO_3)$ (17). Methyl triflate (22 μL, 0.20 mmol) was added to a dark blue solution of **2** (100 mg, 0.167 mmol) in dichloromethane (5 mL), resulting in a rapid color change to dark orange. The resulting solution was layered with hexane (10 mL). After 2 days, filtration, washing with hexane (3 × 1 mL) and drying *in vacuo* yielded the product as brown microcrystals (95 mg, 75%). **^{1}H NMR** (CD$_2$Cl$_2$, 300 MHz): δ 7.56, 7.31 (A$_2$B, ^3J(H−H) = 8.2 Hz, 6H, NAr$H^{3,4,5}$), 2.46 (s, 6H, CCH_3), 1.04 (s, ^2J(Pt−H) = 74.9 Hz, 9H, PtCH_3). **^{13}C NMR** (CD$_2$Cl$_2$, 75 MHz): δ 180.2 (br, *C*=NAr), 139.5 (C^{Ar}), 129.7−129.3 (br m, C^{Ar}), 127.7 (C^{Ar}), 23.4 (C*C*H$_3$), 23.3 (C*C*H$_3$), −4.1−5.6 (br, Pt*C*H$_3$). **Anal.**: calcd for $C_{20}H_{21}N_2O_3F_3SCl_4Pt$: C 31.47, H 2.77, N 3.67. Found: C 31.26, H 2.88, N 3.54. Crystals suitable for XRD were obtained from vapor diffusion of hexane into a freshly prepared solution of **17** in 1:1 dichloromethane/hexane.

(NN)Pt(Me)Cl (20). In a round bottomed Schlenk flask fitted with a Vigreux distillation apparatus, **1** (200 mg, 0.53 mmol) and *trans*-(Me$_2$S)$_2$Pt(Me)Cl (198 mg, 0.53 mmol) were dissolved in THF (20 mL). The flask was heated, resulting in a color change from yellow to dark purple, and the temperature was adjusted so that THF slowly distilled (∼20 mL/h). Heating was continued over a period of 12 h, and THF was regularly added to keep the reaction volume above 10 mL. Filtration, washing with THF (3 × 2 mL) and drying *in vacuo* afforded the product as a dark-purple, microcrystalline solid (196 mg, 60%). **^{1}H NMR** (CD$_2$Cl$_2$, 300 MHz): δ 7.59 (2H), 7.53 (2H), 7.34 (1H), 7.29 (1H) (2 × A$_2$B, ^3J(H−H) = 8.2 Hz, ^3J(H−H) = 8.2 Hz, NAr$H^{3,4,5}$), 1.72 (s, 3H, CCH_3), 1.19 (s, ^4J(Pt−H) = 9.3 Hz, 3H, CCH$_3$), 0.94 (s, ^2J(Pt−H) = 80.8 Hz, 3H, PtCH_3). **^{13}C NMR** (CD$_2$Cl$_2$, 75 MHz): δ 176.2 (*C*=NAr), 174.8 (*C*=NAr), 142.2 (C^{Ar}), 142.0 (C^{Ar}), 129.7 (C^{Ar}), 129.24 (C^{Ar}), 129.18 (C^{Ar}), 128.9 (C^{Ar}), 128.7 (C^{Ar}), 127.9 (C^{Ar}), 21.6 (CCH_3), 20.3 (C*C*H$_3$), −13.4 (Pt*C*H$_3$). **Anal.**: calcd for $C_{17}H_{15}N_2Cl_5Pt$: C 32.95, H 2.44, N 4.52. Found: C 32.64, H 2.50, N 4.51.

$(NN)Pt(Me)(O_3SCF_3)$ (18). A mixture of **20** (12 mg, 19 μmol) and AgOTf (5 mg, 19 μmol) in acetone-d_6 was stirred for 5 min, during which time its color changed from dark purple to orange. A slightly grayish precipitate (AgCl) was removed by filtration, and the resulting orange solution was characterized by ^{1}H NMR spectroscopy. **^{1}H NMR** (CD$_2$Cl$_2$, 300 MHz): δ 7.78 (2H), 7.76 (2H), 7.59 (1H), 7.54 (1H) (2 × A$_2$B, ^3J(H−H) = 8.2 Hz, ^3J(H−H) = 8.2 Hz, NAr$H^{3,4,5}$), 2.32 (s, 3H, CCH_3), 2.15 (s, ^4J(Pt−H) ≈ 11 Hz, 3H CCH_3), 0.57 (s, ^2J(Pt−H) = 74.8 Hz, 3H, PtCH_3).

Thermolysis of 4a and 5a. Equimolar amounts of **2** and AgOTf or CuOTf·1/2C$_7$H$_8$ were dissolved in benzene (3 mL) and heated to 50 °C for 3 days in a closed vessel. The resulting mixture was passed over a short column of aluminum oxide. The undissolved solids were taken in dichloromethane and passed over the same column, which was thoroughly washed with dichloromethane until the washings became colorless. Solvent was evaporated under reduced pressure from the resulting black solution, and the residue was weighed and analyzed by ^{1}H NMR.

UV−Vis Spectroscopy. UV−vis spectra were measured on a Hitachi U-2010 instrument. Samples were prepared in a nitrogen-filled glovebox and introduced into Teflon-stoppered quartz cells with a path length of 1 cm. Measurements involving **2** were performed in benzene, while those involving **3** were conducted in 1:1 dichloromethane/benzene to ensure solubility of the reactants and products. Samples containing AgOTf were prepared by appropriate dilution of ∼2 mM solutions of **2**, **3** and AgOTf. Due to the low solubility of CuOTf, mother solutions were prepared by addition of a weighed amount of CuOTf·1/2C$_7$H$_8$ to 5 mL of a ∼2 mM solution of **2** or **3**. In the case of **2**, this solution is only moderately stable at room temperature and was used within 3 h.

PFG NMR Spectroscopy. Diffusion coefficients were measured by pulsed-field-gradient NMR (PFG NMR) on ∼14 mM solutions in CD$_2$Cl$_2$ at 25 °C using the pulse sequence of Wu et al.,[77] which is based on stimulated echo (STE)[78] and uses longitudinal-eddy-current delay (LDE)[79] and bipolar gradient pulses. The absolute gradient strength was calibrated against 1% H$_2$O in D$_2$O, which has a diffusion coefficient of 18.7 × 10^{-10} m^2 s^{-1}. Diffusion coefficients (D) were extracted using the TOPSPIN[80] program.

Hydrodynamic volumes were calculated as described by Macchioni et al.,[81] using a modified Stokes−Einstein relation:

$$D = \frac{kT}{c(r_{solv}, r_H)\pi\eta r_H} \quad (1)$$

where $\eta = 4.23\cdot 10^{-4}$ Pa·s is the viscosity of dichloromethane, r_H the hydrodynamic radius of the solute, r_{solv} = 2.49 Å the

(77) Wu, D.; Chen, A.; Johnson, C. S. *J. Magn. Reson. A* **1995**, *115*, 260–264.
(78) Tanner, J. E. *J. Chem. Phys.* **1970**, *52*, 2523–2526.
(79) Gibbs, S. J.; Johnson, C. S. *J. Magn. Reson.* **1991**, *93*, 395–402.
(80) *TOPSPIN*, 2.1.1; Bruker: Rheinstetten, 2008.
(81) Macchioni, A.; Ciancaleoni, G.; Zuccacia, C.; Zuccacia, D. *Chem. Soc. Rev.* **2008**, *37*, 479–489.

Table 5. Crystallographic Data for Compounds **4a**, **5b**, and **6a**

	4a	5b	6a
chem formula	$C_{19}H_{18}Cl_4CuF_3N_2O_3PtS$	$C_{50}H_{48}Ag_2Cl_8F_6N_4O_6Pt_2S_2$	$C_{57}H_{44}Cl_8CuF_3N_4O_3Pt_2S$
FW	811.86	1868.56	1659.4
cryst syst	triclinic	triclinic	monoclinic
space group	$P\bar{1}$	$P\bar{1}$	$C2/c$
a [Å]	9.2087(4)	10.6556(12)	19.8903(4)
b [Å]	10.9551(5)	12.1622(13)	18.8114(5)
c [Å]	14.8595(8)	12.6936(13)	17.0905(3)
α [deg]	110.493(3)	110.231(12)	90.00
β [deg]	92.371(3)	105.478(11)	110.0366(13)
γ [deg]	108.700(2)	90.209(10)	90.00
V [Å^3]	1309.98(11)	1479.2(3)	6007.6(2)
Z	2	1	4
D_{calcd} [g cm^{-3}]	2.058	2.098	1.835
F(000)	776	896	3208
μ [mm^{-1}]	6.679	5.868	5.443
temp. [K]	173	220	203
wavelength [Å]	0.71073	0.71070	0.71073
measd rflns	14635	12197	18502
unique rflns	5959	6777	6866
data/restraints/param	5959/0/311	6777/0/366	6866/7/356
R(F) ($I > 2\sigma(I)$)	0.0816	0.0302	0.0381
wR(F^2) ($I > 2\sigma(I)$)	0.2013	0.0786	0.1085
GOF	1.174	1.026	0.860

hydrodynamic radius of dichloromethane, and $c(r_{solv},r_H)$ a correction factor that accounts for the relative size of the solvent and solute molecules. We used the expression of $c(r_{solv},r_H)$ introduced by Chen:[82]

$$c = \frac{6}{1 + 0.695\left(\frac{r_{solv}}{r_H}\right)2.234} \qquad (2)$$

ESI-MS. ESI-MS spectra were recorded on a ThermoFinnigan TSQ Quantum instrument. Ions with masses above 1500 were studied on a Finnigan TSQ700 instrument. CID spectra were measured using argon as collision gas.

{[(NN)PtR$_2$]M(NCMe)}$^+$ and{ [(NN)PtR$_2$]$_2$M}$^+$ (R = Me, Ph; M = Cu, Ag) were electrosprayed from solutions freshly prepared as follows: [(NN)PtR$_2$] (∼1 mg) and MOTf (∼1 mg) were dissolved in acetonitrile (2 mL), and the resulting solution was diluted 20 times.

X-ray Crystallography. Relevant details about the structure refinements are given in Tables 5 and 6, and selected geometrical parameters are included in the captions of the corresponding figures. Data collection was performed on a Bruker-Nonius Kappa-CCD (graphite monochromator, Mo Kα). The structures were solved by direct methods[83] and refined by full-matrix least-squares analysis.[84] All non-H atoms were refined anisotropically unless otherwise stated in the figure caption. Hydrogen atomic positions are based on stereochemical considerations. The disordered $CF_3SO_3^-$ anions in structures **6a** and **11b** were refined over two positions.

DFT Calculations. Geometry optmizations were performed using the Gaussian03 package.[85] The BP86 exchange-correlation functional was employed. The Stuttgart/Dresden[62,63] basis set and effective core potential were used for transition metals, along with a 6-31+G(d) basis set on all other atoms. Diffuse functions on main group elements were found to be necessary for an accurate description of structure **7a** and thus were included for all calculations performed with the Gaussian03 program. Due to the flat character of the potential energy surfaces encountered, the GDIIS algorithm was used systematically and "tight" convergence criteria were imposed. In one case (structure **9a2**), "tight" convergence could not be achieved, and only convergence with the normal criteria was obtained. A full frequency calculation was performed on each structure to ensure that they are true minima.

Energy partitioning analyses[66] were performed with the ADF2008 package[86−88] on geometries optimized as described above. The BP86 exchange-correlation functional was used, and scalar relativistic effects were included *via* the zeroth order regular ap-

Table 6. Crystallographic Data for Compounds **11b** and **12**

	11b	12
chem formula	$C_{48}H_{40}Ag_2Cl_4F_6N_2O_6PtS_2$	$C_{34}H_{28}Cl_{10}Cu_3F_9N_2O_9PtS_3$
FW	1471.59	1616.035
cryst syst	orthorhombic	triclinic
space group	*Pnma*	$P\bar{1}$
a [Å]	26.1863(5)	12.6180(2)
b [Å]	19.3506(3)	12.8711(3)
c [Å]	10.1987(2)	17.6498(4)
α [deg]	90.00	77.4279(11)
β [deg]	90.00	80.5915(10)
γ [deg]	90.00	69.5194(9)
V [Å^3]	5167.9(2)	2608.91(9)Å^3
Z	4	2
D_{calcd} [g cm^{-3}]	1.891	2.057
F(000)	2864	1564
μ [mm^{-1}]	3.809	4.59
temp. [K]	223	223
wavelength [Å]	0.71073	0.71073
measd rflns	23572	36432
unique rflns	5988	11895
data/restraints/param	5988/0/332	11895/0/642
R(F) ($I > 2\sigma(I)$)	0.0517	0.0522
wR(F^2) ($I > 2\sigma(I)$)	0.1608	0.1432
GOF	1.079	1.033

(82) Chen, H.-C.; Chen, S.-H. *J. Phys. Chem.* **1984**, *88*, 5118–5121.
(83) Altomare, A.; Burla, M.; Camalli, M.; Cascarano, G.; Giacovazzo, C.; Guagliardi, A.; Moliterni, A.; Polidori, G.; Spagna, R. *J. Appl. Crystallogr.* **1999**, *32*, 115–119.
(84) Sheldrick, G. M. *SHELXL-97 Program for the Refinement of Crystal Structures*; University of Goettingen: Germany, 1997;
(85) Frisch, M. J.; et al. *Gaussian 03*, Revision D.01; Gaussian, Inc.: Wallingford, CT, 2004.
(86) te Velde, G.; Bickelhaupt, F. M.; van Gisbergen, S. J. A.; Fonseca Guerra, C.; Baerends, E. J.; Snijders, J. G.; Ziegler, T. *J. Comput. Chem.* **2001**, *22*, 931–967.
(87) Fonseca Guerra, C.; Snijders, J. G.; te Velde, G.; Baerends, E. J. *Theor. Chem. Acc.* **1998**, *99*, 391.
(88) *ADF2008. 01, SCM*, Theoretical Chemistry.Vrije Universiteit: Amsterdam, The Netherlands, 2008; http://www.scm.com.

proximation (ZORA) formalism. A TZ2P basis set was used and the electrons up to 1s for C, N, O, F, 2s for S and Cl, 3s for Cu, 4s for Ag, and 5d for Pt were treated within the frozen core approximation. The total bond energy is divided in two parts (eq 3):

$$\Delta E = \Delta E_{\text{prep}} + \Delta E_{\text{int}} \quad (3)$$

where ΔE_{prep} (positive) is the energy required to deform the fragments from their optimized geometries to the geometry they adopt in the complex, and ΔE_{int} (negative) is the actual change in energy that occurs when the fragments are combined together in the complex. ΔE_{int} can be divided further according to eq 4:

$$\Delta E_{\text{int}} = \Delta E_{\text{Pauli}} + \Delta E_{\text{elstat}} + \Delta E_{\text{orb}} \quad (4)$$

where ΔE_{Pauli} (positive) accounts for the destabilizing interactions between occupied orbitals and can be related to steric repulsion, ΔE_{elstat} (negative) corresponds to the electrostatic interaction between the prepared fragments before relaxation of the electron density, and ΔE_{orb} (negative) is the change in energy occurring when the electron density is allowed to relax to the minimal energy. This last term contains both charge transfer (the donor−acceptor interactions between occupied orbitals of one fragment and unoccupied orbitals of the other) and polarization contributions (the interactions between empty and filled orbitals of a single fragment caused by the presence of the other). The charges associated to each fragment were computed by the Hirshfeld[89] method.

Acknowledgment. We acknowledge support from the Swiss National Foundation. We thank Dr. B. Schweizer and Mr. P. Seiler for the XRD structure determinations and Dr. M.-O. Ebert for assistance with the PFG NMR diffusion measurements.

Supporting Information Available: X-ray crystallographic data in CIF format, ORTEP representations of the structures of **7a** and **17**, UV−vis data relative to the solvatochromism of **2** and **3**, ^{1}H NMR data relative to the interaction of **3** and AgOTf, experimental and fitted isotope patterns for methyl scrambling experiments, *XYZ* coordinates for DFT-optimized geometries, and complete reference 85 (ref 2 in SI).This material is available free of charge via the Internet at http://pubs.acs.org.

JA900449Y

(89) Hirshfeld, F. L. *Theor. Chim. Acta* **1977**, *44*, 129–138.